

ELASTODYNAMIC GREEN'S TENSOR IN ANISOTROPIC MEDIUM

A Thesis

Presented to

the Department of Earth and Atmospheric Sciences

University of Houston

In Partial Fulfillment

of the Requirements for the Degree

Master of Science

By

Zhao Li

August 2013

ELASTODYNAMIC GREEN'S TENSOR IN ANISOTROPIC MEDIUM

Zhao Li

APPROVED:

Dr. Evgeny M. Chesnokov, Chairman

Department of EAS

Dr. Donald J. Kouri,

Department of Physics

Dr. Aibing Li,

Department of EAS

Dr. Dan Wells, Dean

College of Natural Sciences and Mathematics

Acknowledgements

First of all, I would like to thank my parents for supporting me both mentally and financially during the past two years.

I would like to express appreciation to my advisor Dr. Evgeny Chesnokov: for his support, guidance, and wisdom during the past two years for my research at the University of Houston. He has always been supportive, giving constructive suggestions, and willing to discuss all the details of my thesis study. Without him, I can never achieve this piece of work.

I want to thank my committee members: Dr. Donald Kouri and Dr. Aibing Li. They have helped me a lot for understanding general physics and geophysics ideas as well as giving insightful suggestions throughout.

I also want to thank the students in EAS department: Aslan Gassiyev, Rui Zhou, Tao Jiang, Xin Zhang, and Xinglu Lin, for discussion and providing so many help during my study at U of H.

ELASTODYNAMIC GREEN'S TENSOR IN ANISOTROPIC MEDIUM

An Abstract of a Thesis

Presented to

the Department of Earth and Atmospheric Sciences

University of Houston

In Partial Fulfillment

of the Requirements for the Degree

Master of Science

By

Zhao Li

August 2013

Abstract

This thesis is dedicated to study the elastodynamic Green's tensor in anisotropic medium in order to understand the influence of anisotropy on the point source radiation.

In the first part of this thesis, a new form of elastodynamic Green's tensor in VTI medium is found based on the method of Tsvankin and Chesnokov (1990). I found the analytical asymptotic Green's tensor for elliptical anisotropic medium. I propose a new form of approximated qP-qSV solution for weak TI medium while the solution of SH wave can always be found analytically. The new form of the Green's tensor is uniform through all directions. The accuracy of the approximated results will decrease as Thomsen parameters increase.

In the second part, I study the anisotropic effect due to initial stress on the Green's tensor. A six-rank tensor introduced by Nikitin and Chesnokov (1981) is being used to describe the effect of deviatoric stress on the symmetry of the medium. The Green's tensor in general anisotropic medium is calculated. I studied four types of uniaxial initial stress. The phase velocity and radiation patterns in the pre-stress medium are calculated. Last, I examine the error brought by the approximation in calculating the Green's tensor.

Table of Contents

Acknowledgements	iii
Abstract	v
Review and motivation	1
Part I,	4
Elastodynamic Green's tensor in VTI medium	4
1. The setting of the problem	4
1.1 The elastic wave equation	4
1.2 The procedure to solve dynamic green's tensor	6
2. The stiffness tensor and other property of VTI medium	8
2.1 The stiffness tensor	8
2.2 Phase velocity	9
2.3 Thomsen parameters	13
2.4 Group velocity	14
3. Green's tensor	16
3.1 The isotropic case	16
3.2 VTI case	17
4. Synthetic results – radiation patterns and synthetic seismogram	33
4.1 Radiation patterns	33
4.2 Synthetic seismograms in the homogeneous media	55
5 Conclusion of Part I	65
Part II	66
Green's tensor in pre-stressed medium	66
6 The setting of the problem	67
6.1 Wave equation in pre-stressed medium	67
6.2 Calculation of the Green's tensor	71
7 Green-Christoffel and the plane wave in pre-stressed medium	74
7.1 Stiffness tensor	74
7.2 Phase velocity	75
7.3 Calculated velocities for different models	76
8 Synthetic results – radiation patterns and synthetic seismograms	83
8.1 Radiation patterns	83
8.2 Synthetic seismogram	86
9 Conclusion for Part II	94
10 Reference	95

Review and motivation

In the field of exploration seismology, people rely on the seismic wave propagation to see the earth's interior. One of the most interesting problems is how the wave propagated in different type of media, which is also known as the forward problem. The forward problem is that given the information about the source and medium then to calculate the elastic wave field.

Elastodynamic Green's tensor is the solution of the elastic wave equation with a point source. It is a second-rank tensor. The columns are related with the three components of the displacement and the rows are related with the three components of the source. Elastodynamic Green's tensor in isotropic medium has been solved analytically for a long time. The point-source solution in an isotropic unbounded medium was first solved by Stokes (1849). This well-known result is actually the elastodynamic Green's tensor in isotropic medium.

The problem of wave propagation in anisotropic media has been gained more and more attentions throughout the last century. For the general anisotropic cases, the Green's tensor is usually calculated numerically. One of the most common ways to solve Green's tensor is to present it in an integral formula. The integral can be solved by asymptotic expansions like stationary phase approximation (SPA).

Ben-Menahem and Sena (1990) has solved the asymptotic dyadic Green's tensor based

on the stationary phase method. Their analytic solution yields a simplification of the slowness in elliptical anisotropy.

Vavrycuk *et al.* has published several studies (1996, 1997, 2002) regarding the anisotropic Green's tensor. Rather than using SPA, he involved high-order ray expansion to find the analytical formula for the near-field. However, this method will encounter problems at the directions where the phase velocity of the shear waves equals each other. Vavrycuk (2002) and Gridin (2000) have studied this problem in different ways. Generally, it uses higher-order approximations with additional terms. The ray theory will collapse at the shadow zones; therefore, it is unable to model the wave field in the complicated structures.

Tsvankin and Chesnokov (1990) simplified the integral transform by using low-order Fourier series to approximate the azimuthally dependent property of Green's tensor in general anisotropic medium. This method provides a semi-analytical way to calculate the Green's tensor in a very fast time. It is not affected by the problem at shear wave singularities described above. Tsvankin (1995) had proposed a way to find the analytical radial components of Green's tensor in weak VTI medium. However, to the author's understanding, the approximation is not linear and has a vibrating nature that will affect the results.

Since the property of the VTI medium is not changing with the azimuth angle, the procedure described in Tsvankin and Chesnokov (1990) can be further simplified. In the first part of this thesis, I find a new analytical form of the complete Green's tensor in VTI medium based on this method.

The second part of the thesis is related with one of the special cause for the anisotropy – the initial stress. The effect of the static initial stress on elastic wave propagation has been studied by various authors. Biot (1940) use a special stress tensor to study the effect of initial stress on the elastic wave propagation. Dahlen (1972) developed the theory about the pre-stressed medium but was proved later by Nikitin (1984) as one of the special case of the general theory.

Nikitin and Chesnokov (1981) studied the effect of initial stress by considering an additional six-rank tensor which is related with the initial deviatoric stress. The symmetry of the medium will be affect by the deviatoric stress while the strength of the elastic parameters will related with the initial pressure. Considering the case when the background medium is isotropic, the plane wave solution is found via Born approximation when the stress distributed periodically in space (Vshvtsev, 1996).

To the author's understanding, most of the studies in this topic are related to the plane wave propagation. In this thesis, I calculate the Green's tensor by the numerical method described by Tsvankin and Chesnokov (1990). I study not only the phase velocity but also the radiation patterns of a point source generated in the pre-stressed medium.

Part I,

Elastodynamic Green's tensor in VTI medium

In this part of the thesis, I find the analytical solution of elastodynamic Green's tensor in VTI medium. First, the elastic wave equation for Green's tensor is derived. Then, the basics of elastic wave propagation are reviewed. After that, steps for solving the Green's tensor are shown in detail. Three elements of Green's tensor are calculated and studied. The synthetic study of radiation patterns and seismograms are shown at the end of this part of thesis.

1. The setting of the problem

1.1 The elastic wave equation

The elastic wave equation can be derived from Newton's second law, where F_i is the force acting upon the object. m is the mass of the object and a_i is the acceleration.

$$F_i = ma_i$$

For the continual mechanics, the force vector is the summation of body force, surface traction, and source. The mass will be the density at a point in the medium.

$$\rho(\mathbf{r}, t) \frac{\partial^2 u_i(\mathbf{r}, t)}{\partial t^2} = \frac{\partial \sigma_{ij}(\mathbf{r}, t)}{\partial x_j} + f_i^b(\mathbf{r}, t) + f_i(\mathbf{r}, t); \quad i, j = 1, 2, 3;$$

$$\sigma_{ij} = C_{ijkl} \epsilon_{kl}, \quad i, j, k, l = 1, 2, 3$$

The stress and strain excited by the wave propagation can be described by the Hooke's law. Einstein's summation notation is implied. σ_{ij} is the stress tensor and ϵ_{ij} is the strain tensor. C_{ijkl} is the stiffness tensor and u_i is the displacement. Using Hooke's law, the elastic wave equation can be found.

$$\rho(\mathbf{r}, t) \frac{\partial^2 u_i(\mathbf{r}, t)}{\partial t^2} = \frac{\partial}{\partial x_j} C_{ijkl}(\mathbf{r}, t) \frac{\partial u_k(\mathbf{r}, t)}{\partial x_l} + f_i(\mathbf{r}, t)$$

In this case, I eliminate the body force. Since it is supposed to solve the equation in homogeneous medium, the stiffness tensor is not depended on the location, thus can be out of the differential operator. Finally, I get the elastic wave equation in the homogeneous medium (equation 1-1).

$$\rho \frac{\partial^2 u_i(\mathbf{r}, t)}{\partial t^2} - C_{ijkl} \frac{\partial^2 u_k(\mathbf{r}, t)}{\partial x_j \partial x_l} = f_i(\mathbf{r}, t) \quad (1-1)$$

In order to find the general solution which is independent from the source distribution, I

use the relation described in equation 1-2. G_{ij} is the elastodynamic Green's tensor.

$$u_k(\mathbf{r}, t) = G_{km} * f_m = \int_{-\infty}^{\infty} \int_{-\infty}^{\infty} G_{km}(\mathbf{r}, t; \mathbf{r}_0, t_0) f_m(\mathbf{r}_0, t_0) d\mathbf{r}_0 dt_0 \quad (1-2)$$

$$f_i = \delta_{im} f_m = \delta_{im} \int_{-\infty}^{\infty} \int_{-\infty}^{\infty} \delta(\mathbf{r} - \mathbf{r}_0) \delta(t - t_0) f_m(\mathbf{r}_0, t_0) d\mathbf{r}_0 dt_0$$

By the property of Dirac delta, the source can be expanded. Comparing both sides of the equation 1-2, I get the wave equation 1-3 for Green's tensor. δ_{ij} is the Kronecker symbol.

$$\left(\rho \delta_{ik} \frac{\partial^2}{\partial t^2} - C_{ijkl} \frac{\partial^2}{\partial x_j \partial x_l} \right) G_{km}(\mathbf{r}, t; \mathbf{r}_0, t_0) = \delta_{im} \delta(\mathbf{r} - \mathbf{r}_0) \delta(t - t_0) \quad (1-3)$$

Equation 1-3 indicates that the elastodynamic Green's tensor is the response of the point source. In other words, it's the elementary solution of elastic wave equation 1-1. Once equation 1-3 is solved, equation 1-2 can be used to find the displacement field for the general source distribution.

1.2 The procedure to solve dynamic green's tensor

For simplicity, I change the notation of " $\mathbf{r} - \mathbf{r}_0$ " to " \mathbf{r} " and " $t - t_0$ " to " t ". It means that origin of coordinate system has been moved to the source location. In order to solve equation

1-3, I expand the Green's tensor and Dirac delta function into Fourier series. By doing this, I received the wave equation in frequency and wave vector domain (equation 1-4-a).

$$(\rho\delta_{ik}\omega^2 - C_{ijkl}k_jk_l)G_{km}(\mathbf{k}, \omega) = -\delta_{im} \quad (1-4-a)$$

$$k_i = \frac{\omega}{V_i} \quad (1-4-b)$$

k_i is the wave vector (equation 1-4-b), which is also known as spatial frequency. ω is the angular frequency. It can be seen from equation 1-5, that the solution of Green's tensor in k - ω domain can easily be found by calculating the negative inverse matrix of Green-Christoffel matrix GC_{ij} .

$$G_{km} = -(GC)_{km}^{-1} = -\frac{adj(GC_{km})}{\det |GC_{km}|}, \quad GC_{ik} = \rho\delta_{ik}\omega^2 - C_{ijkl}k_jk_l \quad (1-5)$$

To find the bilinear solution of the Green's tensor, the stiffness tensor for VTI medium needs to be involved. The inverse Fourier transform has to be done in order to find the solution in time-space domain.

2. The stiffness tensor and other property of VTI medium

2.1 The stiffness tensor

For VTI medium, the symmetric axis is along the Z-axis (in Cartesian coordinates), which means the property of the medium will not change for different azimuth angles. It is a relative simple type of anisotropic symmetry but is still much more complicated than isotropic case.

First of all, the stiffness tensor of VTI medium has five independent elements rather than two for isotropic medium. Stiffness tensor is defined as the first derivative of stress over strain which correspond the medium's property. It connects the stress and strain tensor via Hooke's law. Stiffness tensor is a fourth rank tensor which has 81 non-zero and 21 independent elements for the general anisotropic medium. It can be written as a compact matrix by considering the symmetry.

$$C_{ij} = \begin{bmatrix} C_{11} & C_{12} & C_{13} & C_{14} & C_{15} & C_{16} \\ C_{21} & C_{22} & C_{23} & C_{24} & C_{25} & C_{26} \\ C_{31} & C_{32} & C_{33} & C_{34} & C_{35} & C_{36} \\ C_{41} & C_{42} & C_{43} & C_{44} & C_{45} & C_{46} \\ C_{51} & C_{52} & C_{53} & C_{54} & C_{55} & C_{56} \\ C_{61} & C_{62} & C_{63} & C_{64} & C_{65} & C_{66} \end{bmatrix}$$

For the isotropic case, the stiffness tensor is controlled by two independent parameters

(λ and μ) known as Lamé parameters.

$$C_{ijkl} = \lambda \delta_{ij} \delta_{kl} + \mu (\delta_{ik} \delta_{jl} + \delta_{il} \delta_{jk})$$

For the VTI medium, the stiffness tensor is more complicated.

$$C_{ijkl} = a \delta_{ij} \delta_{kl} + b (\delta_{ik} \delta_{jl} + \delta_{il} \delta_{jk}) + \gamma \delta_{i3} \delta_{j3} \delta_{k3} \delta_{l3} + d (\delta_{i3} \delta_{j3} \delta_{kl} + \delta_{ij} \delta_{k3} \delta_{l3}) + e (\delta_{il} \delta_{k3} \delta_{j3} + \delta_{jk} \delta_{i3} \delta_{l3} + \delta_{ik} \delta_{j3} \delta_{l3} + \delta_{jl} \delta_{k3} \delta_{i3})$$

“a” and “b” can be interpreted as Lamé parameters. “d”, “e”, and “f” are additional parameters which describe the anisotropy property of the medium.

2.2 Phase velocity

Phase velocity is the velocity perpendicular to the wave-front. The anisotropy will lead to shear wave splitting, which is unique to anisotropic medium. In order to explain this phenomenon, I have to examine the solution of plane wave equation 2-1.

I substitute the general formula of plane wave (equation 2-2) into equation 2-1.

$$\rho \frac{\partial^2 u_i}{\partial t^2} = C_{ijkl} \frac{\partial^2 u_k}{\partial x_j \partial x_l} \quad (2-1)$$

$$u_i = e^{ik(n_i x_i - vt)} \quad (2-2)$$

n_i is the direction vector and v is the phase velocity. Considering the property of Kronecker symbol, equation 2-1 can be rewritten.

$$(\Gamma_{ik} - \rho v^2 \delta_{ik}) u_k = 0 \quad (2-3)$$

$$\Gamma_{ik} = C_{ijkl} n_j n_l$$

Equation 2-3 is Green-Christoffel equation, which is depended upon the property of medium and the direction of phase velocity.

$$|\Gamma_{ik} - \rho v^2 \delta_{ik}| = 0 \quad (2-4)$$

Equation 2-4 is the condition that the plane wave will exist in the homogeneous anisotropic medium. It is a cubic equation of the square of phase velocity which should has three distinct roots correspond to different modes of wave. The eigenvectors of equation 2-3 are the polarizations.

$$2\rho V_p^2 = (C_{11} + C_{44}) \sin^2 \theta + (C_{33} + C_{44}) \cos^2 \theta + K$$

$$2\rho V_{SV}^2 = (C_{11} + C_{44})\sin^2 \theta + (C_{33} + C_{44})\cos^2 \theta - K \quad (2-5-a)$$

$$\rho V_{SH}^2 = C_{66}\sin^2 \theta + C_{44}\cos^2 \theta$$

$$K = \sqrt{((C_{11} - C_{44})\sin^2 \theta - (C_{33} - C_{44})\cos^2 \theta)^2 + 4(C_{13} + C_{44})^2 \sin^2 \theta \cos^2 \theta}$$

These are the eigenvalues of equation 2-4 for VTI medium. θ is the angle between the direction of wave propagation and Z-axis. For the isotropic case, the solutions are much simpler,

$$V_P = \sqrt{\frac{\lambda + 2\mu}{\rho}}$$

$$V_S = \sqrt{\frac{\mu}{\rho}}$$

In isotropic media, two of the phase velocity (SV and SH) equals to each other. The values of phase velocities do not depend on directions. There are only two waves observable which are called P- and S-wave, respectively. P stands for primary since it travels faster. S stands for secondary or shear. The reason is that the phase velocity of S-wave is slower and its polarization is within the plane that perpendicular to the direction of wave propagation.

When two of the eigenvalues equal, the solutions of eigenvector will be ambiguous. As a result, there will be no distinct polarization for the S-wave in isotropic media. On the contrary, the split S-wave in anisotropic medium will show recognizable polarizations in the

seismometer. This is a way that the anisotropic medium can be distinguished from isotropic ones.

For anisotropic cases, especially VTI medium, there are three distinct solutions for equation 2-4. I call them the phase velocities of qP-, qSV-, and SH-waves respectively. Their value only depends on the polar angle θ , recalling the property of transversely isotropic medium.

The three orthogonal eigenvectors can be determined for the most cases in VTI medium. The polarization of qP- and qSV-wave are generally not along the P and SV directions. However, they still lies in the radiation plane which determined by the ray direction and the Z-axis. And the polarization of SH-wave is the same with the one in isotropic medium. For some special directions, two of the roots (qSV and SH) equals to each other. In these directions the Green-Christoffel equation will degenerate and there will be ambiguity in determining the polarization. These directions are called shear-wave singularities. As been proven (Dellinger, 1991), there is at least one shear-wave singularity which is along the Z-axis in VTI medium. The physical reason for this singularity is that the amplitudes of the shear-wave are lies in the same isotropic plane when travelling along the Z-axis; therefore, they will be at the same velocity. The locations of other shear wave singularities are related with the stiffness tensor (Crampin, 1981). The analytical results of the polarization in VTI medium can be found in Daley and Hron (1977).

2.3 Thomsen parameters

Thomsen (1986) proposed a method to simplify the formula of “K” in equation 2-5 and defined three dimensionless parameters ε , γ , and δ to describe the anisotropic property of the media. Along with the vertical P- and S- phase velocities, these five parameters can be an alternative to the stiffness tensor.

Thomsen parameters are listed below.

$$\varepsilon = \frac{C_{11} - C_{33}}{2C_{33}}$$

$$\gamma = \frac{C_{66} - C_{44}}{2C_{44}}$$

$$\delta = \frac{(C_{13} + C_{44})^2 - (C_{33} - C_{44})^2}{2C_{33}(C_{33} - C_{44})}$$

$$V_{p0} = \sqrt{\frac{C_{33}}{\rho}}$$

$$V_{s0} = \sqrt{\frac{C_{44}}{\rho}}$$

The physical meaning of γ can be interpreted as the anisotropic parameters for SH-wave. ε and δ are linked with the anisotropic property of both the qP- and qSV-wave. The equation 2-5-a can be greatly simplified if we expanded the “K” at small ε and δ (Tsvankin, 1996).

$$V_p^2 = V_{p0}^2 [1 + 2\delta \sin^2 \theta + 2(\varepsilon - \delta) \sin^4 \theta]$$

$$V_{SV}^2 = V_{S0}^2(1 + 2\delta \sin^2 \theta \cos^2 \theta + 2\varepsilon \sin^4 \theta) \quad (2-5-b)$$

$$\rho V_{SH}^2 = C_{66} \sin^2 \theta + C_{44} \cos^2 \theta$$

Notice that I do not expand the γ parameter in this study; therefore, the property of SH-wave is not affected by this approximation. Equation 2-5-b is known as the phase velocity in weak-anisotropic media. When two of the Thomsen parameters ($\varepsilon=\delta$) equals, equation 2-5-b can be further reduced.

$$V_P^2 = V_{P0}^2(1 + 2\delta) \sin^2 \theta + V_{P0}^2 \cos^2 \theta$$

$$V_{SV}^2 = V_{S0}^2$$

This special type of medium is known as elliptical anisotropy. It can be seen that the anisotropic effect on qSV-wave phase velocity disappeared. Additionally, there is only one shear-wave singularity which is along the axis of symmetry. The elliptical anisotropy can be interpreted as a more symmetric type of VTI media and will be treated first when I am solving the Green's tensor.

2.4 Group velocity

One of the signatures of anisotropic media is the group or ray velocities are different from the phase velocities. The group velocity is the velocity that energy travels. It is along the

ray direction which is the one connected the receiver with the source. In anisotropic media, since the phase velocity is usually not perpendicular to the wave front, the ray directions will deviant from the phase directions. The ray direction in VTI medium can be calculated from the phase direction by equation 2-6 (Crampin, 1981). The θ_p^n and θ_g^n are the phase and group angle (ray angle), respectively. V_p^n is the phase velocity and η is indicating different wave modes.

$$\mathcal{G}_g^\eta = \mathcal{G}_p^\eta + \arctan\left(\frac{1}{V_p^\eta} \cdot \frac{dV_p^\eta}{d\mathcal{G}_p^\eta}\right) \quad (2-6)$$

For some special types of media, there will be three group velocities of qSV-wave within one group angle. This phenomenon is named as shear-wave triplication and its existing condition can be described by equation 2-7 (Dellinger, 1991) which means that the group angle will decrease while the phase angle is increasing. It will result in a strongly tilted wave front of qSV-wave and the energy participation will be complicated.

$$\frac{d\mathcal{G}_g}{d\mathcal{G}_p} < 0 \quad (2-7)$$

3. Green's tensor

3.1 Isotropic medium

Equation 3-1 and 3-2 are elastodynamic Green's tensor in isotropic medium.

$$G_{ij}(\mathbf{k}, \omega) = \frac{1}{\mu \mathbf{k}^2 - \rho \omega^2} \left[\delta_{ij} - \frac{(\lambda + \mu) k_i k_j}{(\lambda + 2\mu) \mathbf{k}^2 - \rho \omega^2} \right] \quad (3-1) \ \& \ (3-2)$$

$$G_{ij}(\mathbf{r}, t, \mathbf{r}_0, t_0) = \frac{n_i n_j}{4\pi \rho V_p^2 |\mathbf{r} - \mathbf{r}_0|} \delta\left[(t - t_0) - \frac{|\mathbf{r} - \mathbf{r}_0|}{V_p}\right] + \frac{(\delta_{ij} - n_i n_j)}{4\pi \rho V_s^2 |\mathbf{r} - \mathbf{r}_0|} \delta\left[(t - t_0) - \frac{|\mathbf{r} - \mathbf{r}_0|}{V_s}\right] \\ + \frac{(3n_i n_j - \delta_{ij})}{4\pi \rho |\mathbf{r} - \mathbf{r}_0|^3} \cdot (t - t_0) \cdot \left\{ H\left[(t - t_0) - \frac{|\mathbf{r} - \mathbf{r}_0|}{V_p}\right] - H\left[(t - t_0) - \frac{|\mathbf{r} - \mathbf{r}_0|}{V_s}\right] \right\}$$

Function H is Heaviside step function. As can be seen from equation 3-2, the elastodynamic Green's tensor contains both the far- and near- wave field. It has four variables of “ $\mathbf{r}, \mathbf{r}_0, t, t_0$ ”, which are time and space locations of the wave field and source respectively.

The first and second terms on the first line of equation 3-2 correspond to the P- and S-wave at the far-field. The function “ $n_i n_j$ ” and “ $\delta_{ij} - n_i n_j$ ” are related with the polarizations. Dirac delta function indicates the wave front, which is spherical for isotropic media. These two parts are called the far-field because their amplitudes are proportional to $\frac{1}{r}$. They will decay slower than the third part of equation 3-2.

The third part of equation 3-2 is the near-field, which can never be calculated by plane wave equation 2-1. It lies between the P- and S-wave and decays much faster than the

far-field. However, it contains information about the source. Its nature can be interpreted after the Green's tensor is convolved with the source-time function (source wavelet).

$$\begin{aligned}
u_i = & \frac{n_i n_j}{4\pi\rho V_p^2 r} F_j(t - \frac{r}{V_p}) - \frac{(n_i n_j - \delta_{ij})}{4\pi\rho V_s^2 r} F_j(t - \frac{r}{V_s}) \\
& + \frac{(3n_i n_j - \delta_{ij})}{4\pi\rho r^2 V_p} \bar{F}_j(t - \frac{r}{V_p}) - \frac{(3n_i n_j - \delta_{ij})}{4\pi\rho r^2 V_s} \bar{F}_j(t - \frac{r}{V_s}) \quad (3-3) \\
& + \frac{(3n_i n_j - \delta_{ij})}{4\pi\rho r^3} \bar{\bar{F}}_j(t - \frac{r}{V_p}) - \frac{(3n_i n_j - \delta_{ij})}{4\pi\rho r^3} \bar{\bar{F}}_j(t - \frac{r}{V_s})
\end{aligned}$$

The solution is equation 3-3. \bar{F}_1 and $\bar{\bar{F}}_1$ are the integral of the source-time function over time. It can be seen that the near-field can be further decomposed into two parts that proportional to $\frac{1}{r^2}$ and $\frac{1}{r^3}$. The polarization of the near-field is complicated, which has both P and S modes.

The near-field reflects the interaction between the P- and S-wave. It's also depended on the frequency of the source-time function. As the frequency increase, the near-field will become less significant.

3.2 VTI case

In this part, the scheme for solving the elastodynamic Green's tensor is explained and shown analytically for the elliptical and weak anisotropic medium. For the more complicated type of symmetries, the general method will be discussed in part two of the thesis.

3.2.1 In k- ω domain

The dynamic Green's tensor in k- ω domain can be found by calculating the negative inverse matrix of Green-Christoffel tensor (equation 1-5). Since I want to find the formula related with the measurable stiffness tensor C_{ij} , I use equation 1-2 to calculate the displacement field directly. In k- ω domain, convolution will become multiplication.

$$u_i(k, \omega) = G_{ij}(k, \omega) f_j(k, \omega)$$

In this case, the source is supposed to be an impulse in r-t domain thus will be constant throughout the k- ω domain. After incorporated the source component f_i , the Green's tensor can be found.

$$\begin{aligned} u_\alpha = & -\frac{f_\alpha}{2 \det |GC_{ij}|} [\rho^2(\omega^2 - k^2 V_p^2)^2 + \rho^2(\omega^2 - k^2 V_{SV}^2)^2 - k^4((\Gamma_{11} - \Gamma_{33})^2 + 4\Gamma_{13}^2)] \\ & - \frac{1}{\det |GC_{ij}|} k_\alpha k_j f_j \{ (C_{11} - C_{66}) \rho [(\omega^2 - k^2 V_p^2) + (\omega^2 - k^2 V_{SV}^2) - (\omega^2 - k^2 V_{SH}^2)] + [(C_{13} + C_{44})^2 k_3^2 + (C_{11} - C_{66})^2 k_r^2] \} \\ & - \frac{1}{\det |GC_{ij}|} k_\alpha k_3 f_3 (C_{13} + C_{44}) \{ \rho [(\omega^2 - k^2 V_p^2) + (\omega^2 - k^2 V_{SV}^2) - (\omega^2 - k^2 V_{SH}^2)] + [(C_{33} - C_{44}) k_3^2 + (C_{12} + C_{44}) k_r^2] \} \end{aligned}$$

(3-6)

$$\begin{aligned}
u_3 &= -\frac{f_3}{\det |GC_{ij}|} (\rho\omega^2 - k^2\Gamma_{11})(\rho\omega^2 - \rho k^2 V_{SH}^2) \\
&\quad - \frac{k_3 k_j f_j}{\det |GC_{ij}|} (C_{13} + C_{44}) \{ \rho [(\omega^2 - k^2 V_P^2) + (\omega^2 - k^2 V_{SV}^2) - (\omega^2 - k^2 V_{SH}^2)] + \\
&\quad + [(C_{33} - C_{44})k_3^2 + (C_{12} + C_{44})k_r^2] \} \\
\det |GC_{km}| &= -\rho^3 (k^2 V_P^2 - \omega^2)(k^2 V_{SV}^2 - \omega^2)(k^2 V_{SH}^2 - \omega^2) \\
\alpha &= 1, 2 \quad j = 1, 2
\end{aligned} \tag{3-7}$$

The phase velocities can be found by equation 2-5-a, which can also be written as equation 3-8-a, 3-8-b, and 3-8-c.

$$V_P = \left\{ \frac{1}{\rho} \left(\frac{\Gamma_{11} + \Gamma_{33}}{2} + \sqrt{\left(\frac{\Gamma_{11} - \Gamma_{33}}{2} \right)^2 + \Gamma_{13}^2} \right) \right\}^{\frac{1}{2}} \tag{3-8-a}$$

$$V_{SV} = \left\{ \frac{1}{\rho} \left(\frac{\Gamma_{11} + \Gamma_{33}}{2} - \sqrt{\left(\frac{\Gamma_{11} - \Gamma_{33}}{2} \right)^2 + \Gamma_{13}^2} \right) \right\}^{\frac{1}{2}} \tag{3-8-b}$$

$$V_{SH} = \left\{ \frac{\Gamma_{22}}{\rho} \right\}^{\frac{1}{2}} \tag{3-8-c}$$

$$\Gamma_{11} = C_{11}n_r^2 + C_{44}n_3^2 \quad \Gamma_{13} = (C_{13} + C_{44})n_r n_3$$

$$\Gamma_{22} = C_{66}n_r^2 + C_{44}n_3^2 \quad \Gamma_{33} = C_{44}n_r^2 + C_{33}n_3^2$$

$$n_r^2 = n_1^2 + n_2^2 = 1 - n_3^2$$

Γ_{ij} only has four radial elements. Equation 3-6 and 3-7 can also be written in the

matrix form.

$$\begin{bmatrix} u_1 \\ u_2 \\ u_3 \end{bmatrix} = \begin{bmatrix} G_{11} & G_{12} & G_{13} \\ G_{21} & G_{22} & G_{23} \\ G_{31} & G_{32} & G_{33} \end{bmatrix} \begin{bmatrix} f_1 \\ f_2 \\ f_3 \end{bmatrix}$$

The elements of elastodynamic Green's tensor in VTI medium are listed below.

$$\begin{aligned} G_{11} &= \frac{-(\rho\omega^2 - C_{44}k_r^2 - C_{33}k_3^2)}{(\rho\omega^2 - \rho k^2 V_p^2)(\rho\omega^2 - \rho k^2 V_{SV}^2)} \cos^2 \varphi - \frac{1}{\rho\omega^2 - \rho k^2 V_{SH}^2} \sin^2 \varphi \\ G_{22} &= \frac{-(\rho\omega^2 - C_{44}k_r^2 - C_{33}k_3^2)}{(\rho\omega^2 - \rho k^2 V_p^2)(\rho\omega^2 - \rho k^2 V_{SV}^2)} \sin^2 \varphi - \frac{1}{\rho\omega^2 - \rho k^2 V_{SH}^2} \cos^2 \varphi \quad (3-9) \\ G_{33} &= -\frac{(\rho\omega^2 - k^2 \Gamma_{11})}{(\rho\omega^2 - \rho k^2 V_p^2)(\rho\omega^2 - \rho k^2 V_{SV}^2)} \\ G_{12} &= \left[\frac{-(\rho\omega^2 - C_{44}k_r^2 - C_{33}k_3^2)}{(\rho\omega^2 - \rho k^2 V_p^2)(\rho\omega^2 - \rho k^2 V_{SV}^2)} + \frac{1}{\rho\omega^2 - \rho k^2 V_{SH}^2} \right] \sin \varphi \cos \varphi \\ G_{13} &= -\frac{k_1 k_3 (C_{13} + C_{44})}{(\rho\omega^2 - \rho k^2 V_p^2)(\rho\omega^2 - \rho k^2 V_{SV}^2)} \\ G_{23} &= -\frac{k_2 k_3 (C_{13} + C_{44})}{(\rho\omega^2 - \rho k^2 V_p^2)(\rho\omega^2 - \rho k^2 V_{SV}^2)} \\ G_{31} &= G_{13} \quad G_{21} = G_{12} \quad G_{32} = G_{23} \end{aligned}$$

For G_{11} and G_{22} , I separate the Green's tensor into qP-qSV part and SH part. It will

leads to severe mistakes if one applied the stationary phase approximation without separating them. Generally speaking, there will be a wrong S-wave and the solution will blow at shear-wave singularities.

3.2.2 Elliptical anisotropy in r-t domain

For the elliptical anisotropy, the problem is largely reduced. Each step of calculation is present and will be discussed in this chapter.

I start from the Green's tensor in k - ω domain (equation 3-9). The next step is to calculate the inverse Fourier transform to take the formula back to time-space domain. Starting from the equation below, there are four integrals for three-dimensional phase wave-number (or slowness) vectors and angular-frequency. The integral is being calculated in cylindrical coordinate system.

$$u_3(r, z, \alpha, t) = \frac{1}{(2\pi)^4} \int_{-\infty}^{\infty} \int_0^{2\pi} \int_{-\infty}^{\infty} \int_0^{\infty} u_3(k_r, k_3, \varphi, \omega) e^{-i[k_r r \cos(\varphi - \alpha) + k_3 z]} e^{i\omega t} k_r dk_r dk_3 d\varphi d\omega$$

I used residue theorem to calculate the integral over k_3 . There are at most six singularities lies in the determinant of Green-Christoffel tensor, which correspond to the qP-, qSV-, and SH-wave propagated upward and downward. If I choose an observation location above the source, there will no downward-propagating wave and vice versa (for the

homogeneous medium). Thus the six singularities of k_3 reduced to three causal ones. According to Jordan's lemma, the path of integral lies in the lower half-space of the complex plane (figure 3-1). The poles of qSV- and SH-wave are shown schematically, their true locations are related with the stiffness tensor. For instance, if C_{44} is less than C_{66} , the phase velocity of the SH-wave will be faster; therefore, the corresponding wave number will be smaller.

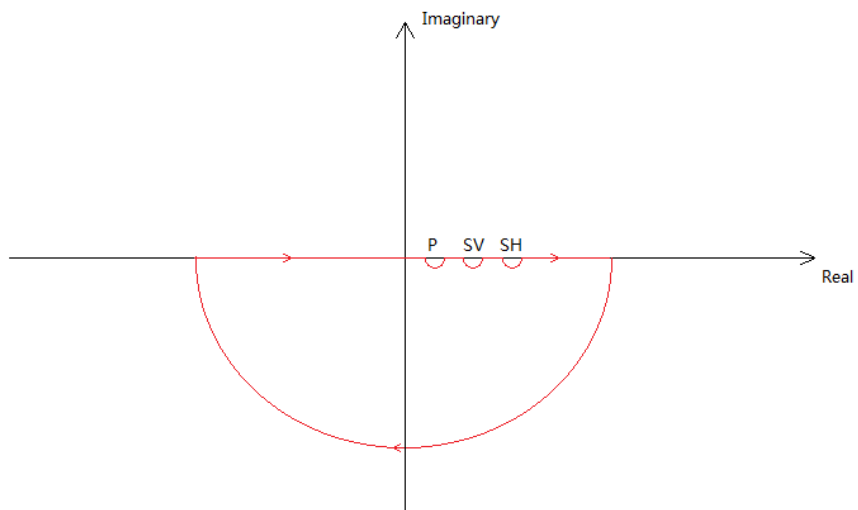


Figure 3-1, Contour of the integral.

The contour detours the singularities. According to Cauchy's residue theorem, the integral will equals zero.

$$\int_{-\infty}^{\infty} dk_3 + \int_{k_P} dk_3 + \int_{k_{SV}} dk_3 + \int_{k_{SH}} dk_3 + \int_{big\ arc} dk_3 = 0$$

As the radius of the big arc goes to infinity, the integral on the big arc will vanish. And the integral over k_3 is depending on the small arcs.

$$\int_{-\infty}^{\infty} dk_3 = -\int_{k_P} dk_3 - \int_{k_{SV}} dk_3 - \int_{k_{SH}} dk_3 - \int_{big\ arc} dk_3 = -\int_{k_P} dk_3 - \int_{k_{SV}} dk_3 - \int_{k_{SH}} dk_3$$

The integral on small arcs can be calculated by the Cauchy principal value integral. Take G_{33} as an example, for the cases when “ $z \geq 0$ ”, the solution will be

$$G_{33} = \frac{i}{2(2\pi)^3} \frac{1}{\rho^2 V_{P0}^2 V_{S0}^2} \left[\frac{(\rho\omega^2 - C_{11}k_r^2 - C_{44}k_P^2)}{2k_P(k_P^2 - k_{SV}^2)} e^{-ik_P|z|} - \frac{(\rho\omega^2 - C_{11}k_r^2 - C_{44}k_{SV}^2)}{2k_{SV}(k_P^2 - k_{SV}^2)} e^{-ik_{SV}|z|} \right] \times \int_0^{2\pi} e^{-ik_r r \cos(\varphi - \alpha)} d\varphi k_r dk_r e^{i\omega t} d\omega$$

(3-10)

$$k_P = \sqrt{\frac{\omega^2}{V_{P0}^2} - (1 + 2\delta)k_r^2} \quad (3-11\ a)$$

$$k_{SV} = \sqrt{\frac{\omega^2}{V_{S0}^2} - k_r^2} \quad (3-11\ b)$$

For parts of downward propagation, the integral can be solved in a similar way.

The two parts in equation 3-10 are related to the qP- and qSV-wave, respectively. There is no SH-wave because that G_{33} corresponds to the force along Z-axis; therefore, there is no excitation in the transverse plane (the plane perpendicular to radial plane within the SH polarization).

Then the integral over azimuth angle can be calculated by the Bessel integral.

$$J_n(x) = \frac{1}{2\pi i^n} \int_0^{2\pi} e^{ix \cos \varphi} \cos(n\varphi) d\varphi$$

$J_n(x)$ is the nth-order Bessel function of the first kind. Considering the property of TI medium and the source component, there will be no Bessel function higher than order-two in the solutions. Substituting the above Bessel integral into equation 3-10, one gets the formula below.

$$G_{33} = \frac{i}{2(2\pi)^2} \frac{1}{\rho^2 V_{P0}^2 V_{S0}^2} \int_{-\infty}^{+\infty} \int_0^{+\infty} \left[\frac{(\rho\omega^2 - C_{11}k_r^2 - C_{44}k_p^2)}{2k_p(k_p^2 - k_{SV}^2)} e^{-ik_p|z|} - \frac{(\rho\omega^2 - C_{11}k_r^2 - C_{44}k_{SV}^2)}{2k_{S1}(k_p^2 - k_{SV}^2)} e^{-ik_{SV}|z|} \right] \times J_0(k_r r) k_r dk_r e^{i\omega t} d\omega$$

I use the stationary phase approximation (Bleistein, 1984) to find the asymptotic solution of the above integral. The Bessel function has the analytical asymptotic formula in equation 3-12.

$$J_n(x) = \sqrt{\frac{2}{\pi k_r r}} e^{-i(k_r r - \frac{n\pi}{2} - \frac{\pi}{4})} \quad (3-12)$$

The stationary phase approximation is a kind of asymptotic expansion at high frequency. For this study, the major part of energy is travelling at the directions close to the ray direction. At other directions, the integral over horizontal slowness gives a vibrating result which will be cancelled if the frequency goes to infinity. The result is the leading far-field terms of the Green's tensor.

The SPA is dedicated to find the asymptotic solution of the integral below.

$$I = \int_a^b f(t) e^{-i\phi(t)} dt$$

A point is called stationary phase point at which the first derivative of the phase function equals zero but the second derivative does not vanishes. The SPP solution can be found by expanding the phase function at these stationary points.

$$I = e^{-i\phi(c)} f(c) \sqrt{-\frac{2\pi}{i|\phi''(c)|}}$$

The stationary horizontal wave-number for qP- and qSV-waves for the elliptical anisotropy are listed below.

$$k_{rp}^{SPP} = \frac{M}{V_{P0}} = \frac{1}{V_{P0}} \left(\frac{r^2}{Br^2 + B^2 |z|^2} \right)^{\frac{1}{2}}$$

$$B = 1 + 2\delta$$

$$k_{rSV}^{SPP} = \frac{\sin \theta}{V_{P0}}$$

After transforming the frequency to time, the final result can be found below.

$$G_{33} = \frac{1}{4\pi} \frac{1}{\rho V_{P0}^2} \left\{ \frac{F_p^{33}(r, z)}{R} \delta \left[t - \frac{1}{V_{P0}} (1 - BM^2)^{\frac{1}{2}} |z| - \frac{1}{V_{P0}} Mr \right] - \frac{F_{SV}^{33}(r, z)}{R} \delta \left[t - \frac{R}{V_{S0}} \right] \right\}$$

(3-13)

$$F_p^{33}(r, z) = \frac{1 - \frac{C_{11}}{C_{33}} M^2 - \frac{C_{44}}{C_{33}} (1 - BM^2)}{\frac{C_{44}}{C_{33}} - 2\delta \frac{C_{44}}{C_{33}} M^2 - 1} \cdot \sqrt{\frac{M(1 - BM^2)^{\frac{1}{2}}}{B \cos \theta \sin \theta}}$$

$$F_{SV}^{33}(r, z) = \frac{1 - \frac{C_{11}}{C_{44}} \sin^2 \theta - \cos^2 \theta}{\frac{C_{44}}{C_{33}} - 2\delta \sin^2 \theta - 1}$$

The above formulas are valid while the source is located at the origin. θ is the polar

angle. The inverse Fourier transform over frequency can also to be evaluated for different types of wavelets.

The dimensionless function F_P^{33} and F_{SV}^{33} are related with the radiation pattern of qP- and qSV-wave. They are indicating the differences between the TI and isotropic Green's tensor. For the isotropic Green's tensor, the radiation pattern only depended on the geometry of the observation (receivers). However, in VTI medium, it's also related with the stiffness tensor of the medium. Even the phase velocity for qSV-wave is isotropic, its amplitude are still affected by the anisotropic property of media.

The "M function" can be interpreted as an anisotropic-weighted sinusoid function. The bracket in the Dirac delta indicates the shape of the wave-front. For the qSV-wave, it is spherical which corresponds to the property of elliptical anisotropy. For the qP-wave, the wave front is depending on the "M function".

The other elements of Green's tensor can be calculated with the same manner. For example, G_{11} in the space and frequency domain are shown in equation 3-14 where α is azimuth angle.

$$G_{11}(r_i, \omega) = G_{11}^{P,SV} + G_{11}^{SH}$$

$$= \frac{\pi}{(2\pi)^3} \frac{\cos^2 \alpha}{C_{33} C_{44}} \frac{1}{R} (F_P^{11} e^{-i(k_P^{SPP} |z| + k_r^{SPP} r)} + F_{SV}^{11} e^{-i(k_{SV}^{SPP} |z| + k_r^{SPP} r)}) + \frac{\pi}{(2\pi)^3} \frac{\sin^2 \alpha}{C_{44}} \frac{1}{R} F_{SH}^{11} e^{-i(k_{SH}^{SPP} |z| + k_r^{SPP} r)}$$

(3-14)

$$F_P^{11} = -C_{33} \frac{1 - \frac{C_{44}}{C_{33}} M^2 - N^2}{N^2 + M^2 - \frac{C_{33}}{C_{44}}} \sqrt{\frac{MN}{B \sin \theta \cos \theta}}; \quad N = (1 - BM^2)^{\frac{1}{2}}$$

$$F_{SV}^{11} = C_{44} \frac{1 - \sin^2 \theta - \frac{C_{33}}{C_{44}} \cos^2 \theta}{\frac{C_{44}}{C_{33}} - (1 + 2\delta) \sin^2 \theta - \cos^2 \theta}$$

$$M_s = \left(\frac{r^2}{B_s r^2 + B_s^2 |z|^2} \right)^{\frac{1}{2}}; \quad B_s = 1 + 2\gamma = \frac{C_{66}}{C_{44}}; \quad N_s = (1 - B_s M_s^2)^{\frac{1}{2}};$$

$$k_{SH}^{SPP} = \frac{M_s}{V_{s0}}$$

As can be seen from equation 3-14, the Green's tensor can be separated as the radial and transverse part which corresponds to the different projection of the force. There are three waves travels at the phase velocity of qP, qSV, and SH, respectively. The "F function" controls the radiation in the vertical plane and the radiation in isotropic plane are depended only on the geometry.

3.2.3 Weak anisotropic case in r-t domain

In this section, I am trying to solve the far-field Green's tensor via SPA in weak-VTI media. Thomsen's parameters are employed to simplify the solution. One important point is that this weak-anisotropic approximation is only focused on qP-qSV part. The SH part can always be solved analytically by the method mentioned in the above section.

I again started from the Green's tensor in k - ω domain and follow the same manner to calculate the integral over vertical wave-number. The difference is that rather writing the dispersion relationship as equation 3-11-a and 3-11-b, I consider the full solution for the general VTI medium. They are written in term of the slowness but not wave-number in order to eliminate the frequency dependency.

$$k = \omega p$$

$$p_\alpha = \sqrt{\frac{0.5}{f-1} \left[(2(\varepsilon+1-f-f\delta)p_r^2 + \frac{1}{V_{p0}^2}(f-2) + \sqrt{4f^2[(\delta+1)^2 - 2\varepsilon - 1] + 8(\varepsilon - \delta - \varepsilon\delta)f + 4\varepsilon^2})p_r^4 + (8f\delta - 4f\varepsilon - 4f^2\delta) \left(\frac{p_r^2}{V_{p0}^2} + \frac{f^2}{V_{p0}^4} \right) \right]}$$

$$p_\beta = \sqrt{\frac{0.5}{f-1} \left[(2(\varepsilon+1-f-f\delta)p_r^2 + \frac{1}{V_{p0}^2}(f-2) - \sqrt{4f^2[(\delta+1)^2 - 2\varepsilon - 1] + 8(\varepsilon - \delta - \varepsilon\delta)f + 4\varepsilon^2})p_r^4 + (8f\delta - 4f\varepsilon - 4f^2\delta) \left(\frac{p_r^2}{V_{p0}^2} + \frac{f^2}{V_{p0}^4} \right) \right]}$$

$$f = 1 - \frac{C_{44}}{C_{33}}$$

Similar to the phase velocity solution (equation 2-5-a), there is a long expression under the square root. After expanding this term at small δ and ε (Thomsen parameters), the dispersion relationships can be simplified.

$$p_\alpha^2 = \frac{1}{V_{p0}^2} - (1 + 2\delta)p_r^2 + 2p_r^4 V_{p0}^2 (\delta - \varepsilon)$$

$$p_\beta^2 = \frac{1}{V_{s0}^2} - \left(1 + 2\frac{\delta - \varepsilon}{f - 1}\right)p_r^2 - 2p_r^4 V_{p0}^2 (\delta - \varepsilon) \quad (3-15 \text{ a \& b})$$

This simplification will not affect the Bessel integral. Taking G_{13} as an example, the

final integral over horizontal slowness can be written as equation 3-16.

$$G_{13}(r_i, \omega) = \frac{\cos \alpha}{8\pi^2} \frac{C_{13} + C_{44}}{C_{33}C_{44}} \int_0^\infty \left[\frac{p_r^2}{2(p_\alpha^2 - p_\beta^2)} e^{-i\omega p_\alpha |z|} - \frac{p_r^2}{2(p_\alpha^2 - p_\beta^2)} e^{-i\omega p_\beta |z|} \right] J_1(\omega p_r r) \omega dp_r \quad (3-16)$$

Expanding the Bessel function at far-field and calculating the first-derivative of the phase function. I found the equation for solving SPPs when neither of z and r equals zeros.

$$16 \frac{z^2}{r^2} V_{p0}^4 (\delta - \varepsilon)^2 p_{rp}^6 - \left[8 \frac{z^2}{r^2} (1 + 2\delta) + 2 \right] (\delta - \varepsilon) V_{p0}^2 p_{rp}^4 + \left[\frac{z^2}{r^2} (1 + 2\delta)^2 + (1 + 2\delta) \right] p_{rp}^2 - \frac{1}{V_{p0}^2} = 0$$

$$16 \frac{z^2}{r^2} V_{p0}^4 (\delta - \varepsilon)^2 p_{rs}^6 + \left[8 \frac{z^2}{r^2} \left(1 + 2 \frac{\delta - \varepsilon}{f - 1} \right) + 2 \right] (\delta - \varepsilon) V_{p0}^2 p_{rs}^4 + \left[\frac{z^2}{r^2} \left(1 + 2 \frac{\delta - \varepsilon}{f - 1} \right)^2 + \left(1 + 2 \frac{\delta - \varepsilon}{f - 1} \right) \right] p_{rs}^2 - \frac{1}{V_{s0}^2} = 0$$

(3-17-a & 3-17-b)

Since I am trying to find the square of the slowness, the above equations are cubic ones and they can be solved analytically. Among the three solutions, only the one with real value has physical meaning and can be used in SPA solution.

When “z=0”, the above equations reduced to:

$$2(\delta - \varepsilon) V_{p0}^2 p_{rp}^4 + (1 + 2\delta) p_{rp}^2 - \frac{1}{V_{p0}^2} = 0$$

$$(\delta - \varepsilon) V_{p0}^2 p_{rs}^4 + \left(1 + 2 \frac{\delta - \varepsilon}{f - 1} \right) p_{rs}^2 - \frac{1}{V_{s0}^2} = 0$$

It is equivalent to equations (3-15). For the case when “r = 0”, the SPPs are set to zeros to be physically meaningful.

After finding the SPP and substitute them into equation 3-16, I can get the approximated analytical solution for weak-VTI media (equation 3-18). Equation 3-17-a and 3-17-b can also be evaluated by numerical methods like Newton-Raphson method.

$$\begin{aligned}
G_{13}(r_i, \omega) &= \frac{\cos \alpha}{8\pi^2} \frac{C_{13} + C_{44}}{C_{33}C_{44}} [F_\alpha(p_{rp})e^{-i\phi_\alpha(p_{rp})} - F_\beta(p_{rs})e^{-i\phi_\beta(p_{rs})}] \\
F_\alpha(p_r) &= \frac{p_r^2}{(p_\alpha^2 - p_\beta^2)} \sqrt{\frac{\omega}{rp_r |\phi_\alpha''(p_r)|}} \\
F_\beta(p_r) &= \frac{p_r^2}{(p_\alpha^2 - p_\beta^2)} \sqrt{\frac{\omega}{rp_r |\phi_\beta''(p_r)|}} \\
\phi_\alpha(p_r) &= \omega(p_r r + p_\alpha |z|) \\
\phi_\beta(p_r) &= \omega(p_r r + p_\beta |z|) \\
\phi_\alpha''(p_r) &= \frac{|z| \omega}{p_\alpha^3} \left[\frac{1+2\delta}{V_{p0}^2} - 12p_r^2(\delta - \varepsilon) + 6V_{p0}^2 p_r^4 (1+2\delta)(\delta - \varepsilon) - 8V_{p0}^4 p_r^6 (\delta - \varepsilon)^2 \right] \\
\phi_\beta''(p_r) &= \frac{|z| \omega}{p_\beta^3} \left[\frac{1+2\delta_s}{V_{s0}^2} + 12 \frac{C_{33}}{C_{44}} p_r^2 (\delta - \varepsilon) - 6V_{p0}^2 p_r^4 (1+2\delta_s)(\delta - \varepsilon) - 8V_{p0}^4 p_r^6 (\delta - \varepsilon)^2 \right] \\
\delta_s &= \frac{\delta - \varepsilon}{f - 1}
\end{aligned}$$

(3-18-1)

The apparent singularities when z or r equals zero can be removed by L'Hopital rule.

The accuracy of the weak-VTI-approximated stationary points is depending on the elastic property of the media. The solutions will be accurate when equation 3-15 is not too far away from the exact one. For some directions (θ), the small deviant of the SPP may lead to big error for the qSV-wave radiation pattern due to the unphysical value of the stationary phase slowness. The accuracy of this approximation will be discussed in detail in the next section.

Besides, SPA may not be a good way to model the strongly distorted wave-front like shear-wave triplication which will happen in TI media (Tsvankin, 1995). For this type of media, the numerical solution is suggested and will be discussed on the following chapters.

Equation 3-18 is the Green's tensor in r-t domain where $p_{\alpha p}$ and $p_{\beta s}$ are the stationary vertical slowness calculated by the dispersion relationship.

$$G_{13}(r_i, t) = \frac{\cos \alpha}{8\pi^2} \frac{C_{13} + C_{44}}{C_{33} C_{44}} [F_{\alpha}(p_{rp}) \delta(t - p_{rp} r - p_{\alpha p} |z|) - F_{\beta}(p_{rs}) \delta(t - p_{rs} r - p_{\beta s} |z|)]$$

(3-19)

The other elements of Green's tensor can be calculated in the same manner. For G_{23} , G_{22} , and G_{12} , the only differences with G_{13} and G_{11} are the projection of the displacement in the isotropic plane (equation 2-9). Thus they will not be shown in this thesis.

4. Synthetic results – radiation patterns and synthetic seismogram

In this section, the radiation patterns and synthetic seismograms calculated from the above analytical solution are shown. First of all, the isotropic cases are shown. Then the exact far-field analytical solution of the elliptical anisotropy is shown and compared with the isotropic solutions. At last, the approximated far-field solution for weak-anisotropic media is presented and its property will be discussed in detail.

4.1 Radiation patterns

4.1.1 Introduction and lobe plots

In this thesis, the definition of radiation pattern is limited to the amplitude generated by the unit force at the unit distance from the point force. Using the isotropic Green's tensor as an example, the radiation pattern will be the argument in front of the Dirac delta function and is shown below for the P-wave part of G_{33} .

$$RP_{33p} = \frac{n_3^2 f_3}{4\pi\rho V_p^2} \quad (4-1)$$

For the physical interpretation, I need to refer to figure 4-1. Remembering the definition of the Green's tensor, G_{33} is responsible for the vertical displacement generated by the

vertical force. As can be seen from figure 4-1, the vertical force is f_3 while n_i is the vector of ray direction. The first n_3 is to project the vertical force f_3 into the ray direction (P-wave). Then the second n_3 is to project the “P-wave-force” back to the vertical axis which is related with the vertical displacement u_3 .

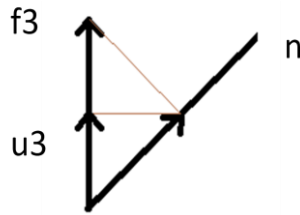


Figure 4-1, Relationship between the source and the radiation patterns.

Similarly, the expression for radiation patterns in elliptical anisotropic Green’s tensor can be found from equation 3-14 and 3-15.

The elliptical anisotropic stiffness tensor (equation 4-2) is obtained by Gajewski (Gajewski, 1993). The stiffness tensor for the compared isotropic media is calculated via the simple average method presented in the same paper.

$$C_{ij} = \begin{bmatrix} 3.52 & 2.68 & 2.03 & 0 & 0 & 0 \\ 2.68 & 3.52 & 2.03 & 0 & 0 & 0 \\ 2.03 & 2.03 & 2.02 & 0 & 0 & 0 \\ 0 & 0 & 0 & 0.31 & 0 & 0 \\ 0 & 0 & 0 & 0 & 0.31 & 0 \\ 0 & 0 & 0 & 0 & 0 & 0.42 \end{bmatrix} GPa \quad (4-2)$$

$$\delta = 0.3706$$

$$\varepsilon = 0.3717$$

$$\rho = 1.8 \text{ g / cc}$$

$$V_{PI} = \sqrt{\frac{(C_{11} + C_{22} + C_{33})}{3\rho}}$$

$$V_{SI} = \sqrt{\frac{(C_{44} + C_{55} + C_{66})}{3\rho}}$$

The radiation patterns of P- and S-waves for isotropic G_{33} , G_{11} , and G_{13} are plotted versus the polar angle in Figure 4-2-a, 4-2-b, and 4-2-c. The elliptical anisotropic cases are plotted in Figure 4-3-a, 4-3-b, and 4-3-c. It can be seen that the anisotropic radiation patterns are not far from the isotropic one. However, even the phase velocity of the qSV-wave is isotropic; its amplitude still behaves differently. This is resulted from the tilted polarization of the qSV-wave. These results are well-agreed with the ones obtained by Gajewski (1993).

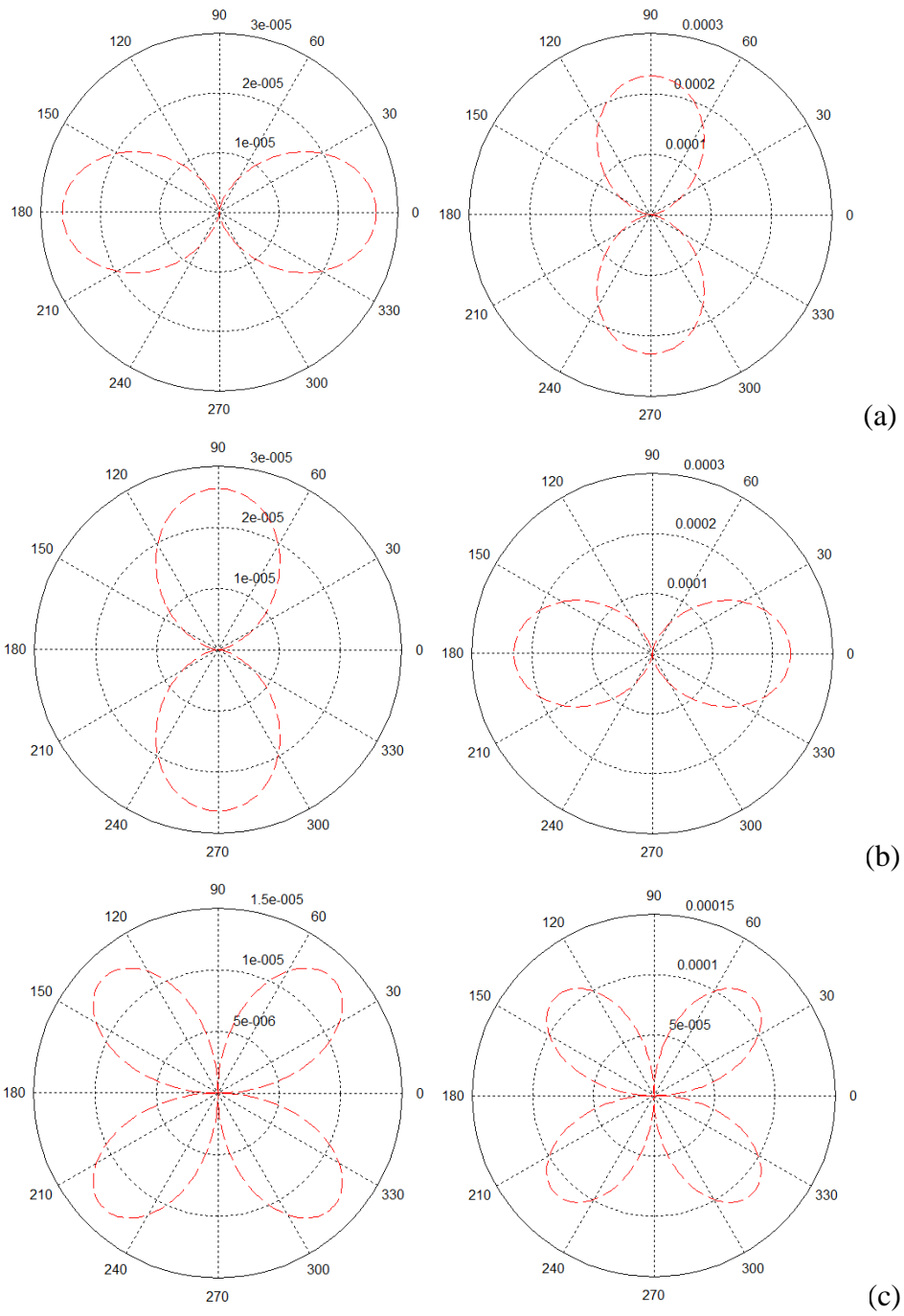


Figure 4-2, Isotropic radiation patterns: the P- and S-wave are on the left and right.

(a)- G_{33} , (b)- G_{11} , and (c)- G_{13} .

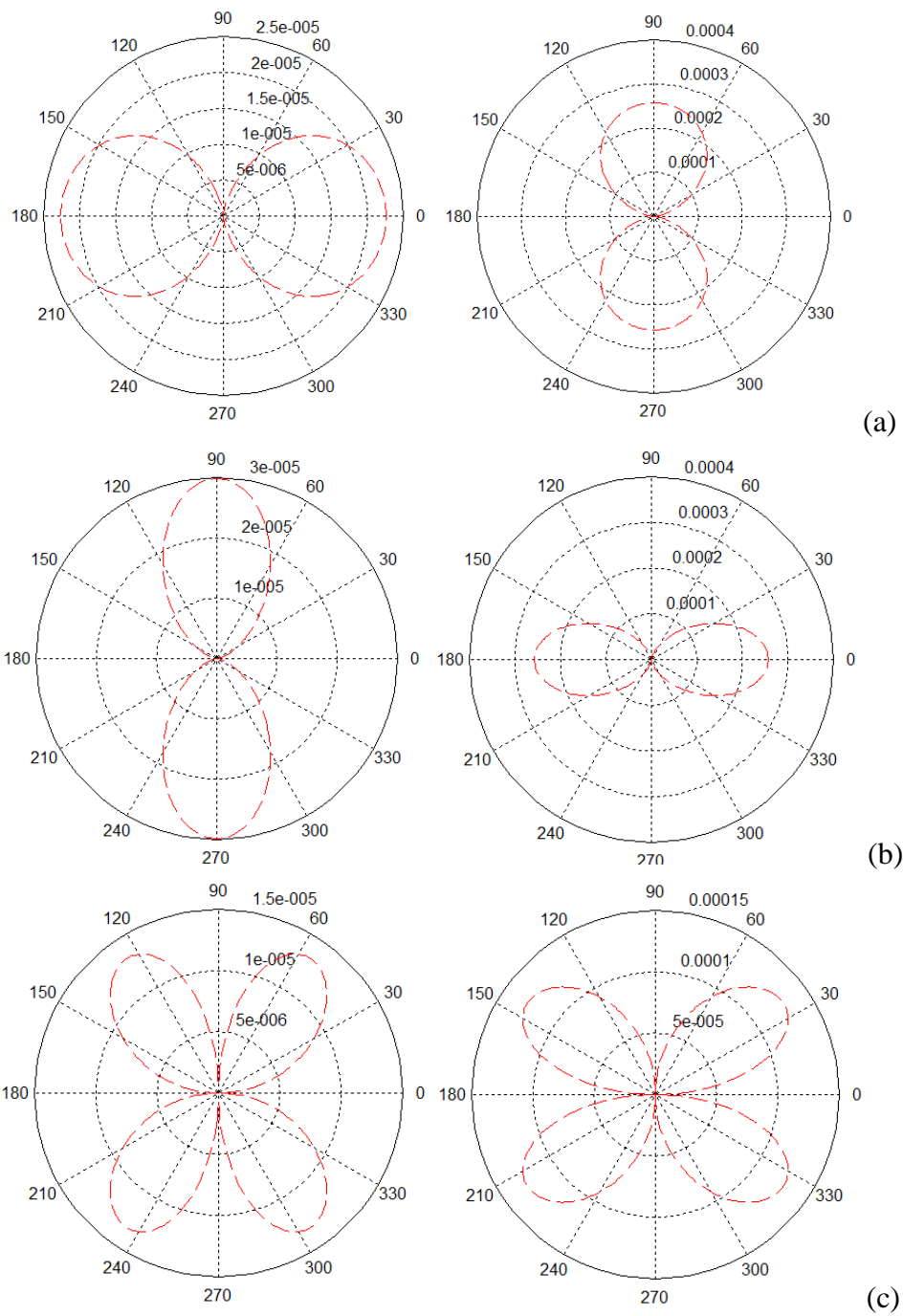


Figure 4-3, Radiation patterns of elliptical anisotropy; the P- and S-wave are on the left and

right. Azimuth angle equals zero.

From figure 4-3, the lobes for vertical displacements are slightly “fatter” while the horizontal displacements are “slimmer” than the isotropic cases (figure 4-2-a and 4-2-b). This is result from the amplitude polarizations for qP- and qSV-wave are not along the ray direction but slightly tilted to the vertical axis. For the case when azimuth angle equals thirty degrees, the radiation patterns for qSV- and SH-wave from G_{11} are plotted in figure 4-4. The radiation pattern of SH part is slightly affected by the phase velocity variation along different polar angles.

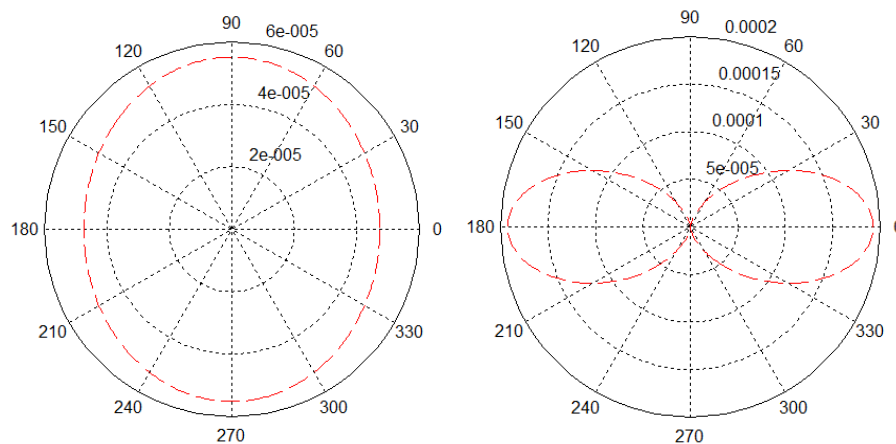


Figure 4-4, Radiation pattern for the SH- (left) and qSV-wave (right)
at 30 degree azimuth.

The stiffness tensor for the weak-anisotropic media is completely empirical (equation 4-3). The radiation patterns of qP- and qSV-wave for G_{33} , G_{11} , and G_{13} are plotted with

polar angle in figure 4-5-a, 4-5-b, and 4-5-c, respectively. Similarly, the radiation patterns of qSV- and SH-wave at thirty degree azimuth are plotted in figure 4-5-d.

$$C_{ij} = \begin{bmatrix} 34.597 & 9.341 & 12.614 & 0 & 0 & 0 \\ 9.341 & 34.597 & 12.614 & 0 & 0 & 0 \\ 12.614 & 12.614 & 30.359 & 0 & 0 & 0 \\ 0 & 0 & 0 & 8.363 & 0 & 0 \\ 0 & 0 & 0 & 0 & 8.363 & 0 \\ 0 & 0 & 0 & 0 & 0 & 12.628 \end{bmatrix} \text{ GPa (4-3)}$$

$$\delta = -0.0328$$

$$\varepsilon = 0.0698$$

$$\rho = 2.5 \text{ g/cc}$$

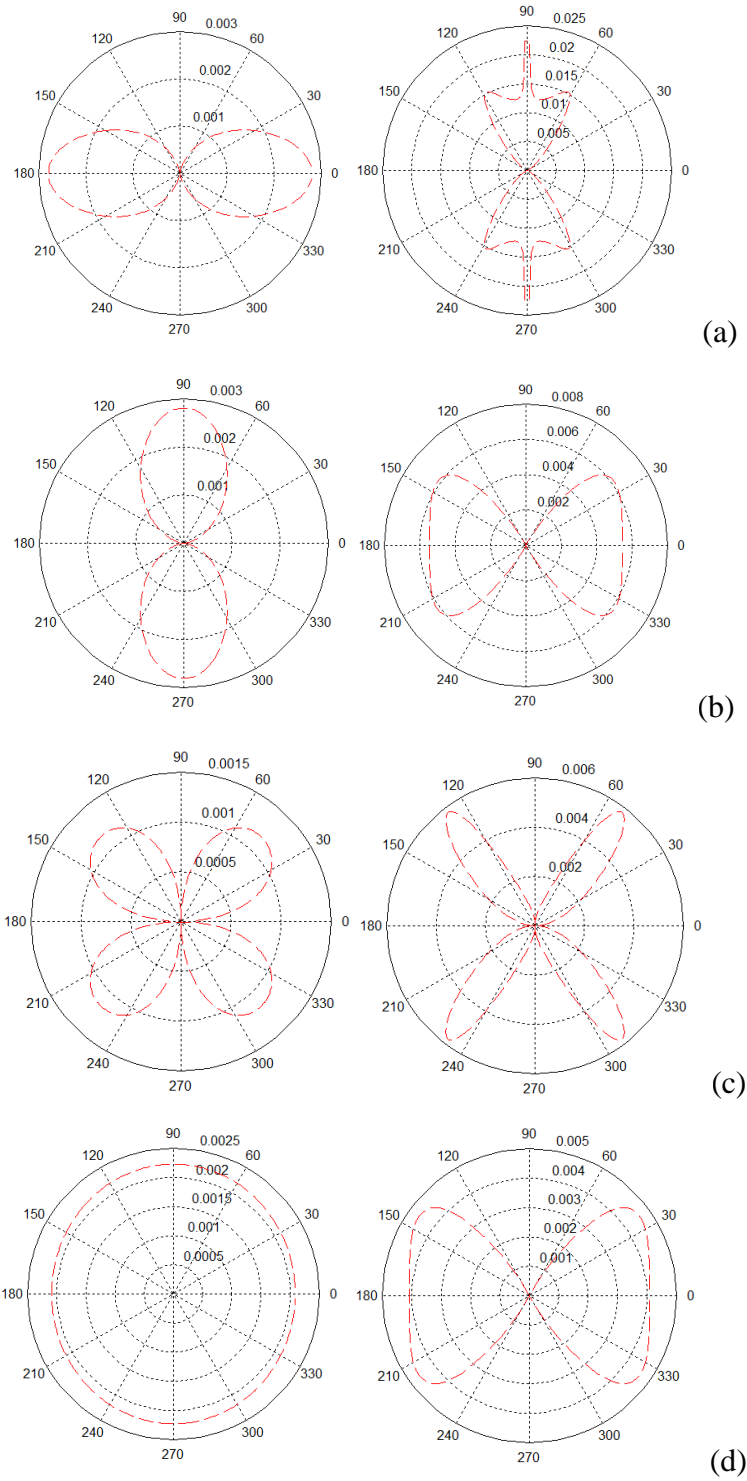


Figure 4-5, Radiation patterns for weak-anisotropic case.

(a)- G_{33} , (b)- G_{11} , (c)- G_{13} , and (d)- G_{11} (qSV- and SH-wave).

4.1.2 Discussions on the radiation patterns in weak VTI media

In this section, I will examine the behavior of the approximated asymptotic solution of the Green's tensor in weak VTI media and to compare them with the numerically calculated results for three different models. First I will study the simplified slowness function (equation 3-15-a and 3-15-b). The approximated dispersion relationship is for the primary interests since it will affect the SPP calculation as well as the second derivative of the phase function and eventually the radiation patterns.

The stiffness tensors of the three models are listed in Table 4-6 while the first model is same as the one in equation 4-3.

Model	C_{11}	C_{33}	C_{44}	C_{66}	C_{13}	Δ	ϵ	σ
#1	34.60	30.36	8.36	12.63	12.61	-0.033	0.070	0.374
#2	34.60	28.36	8.36	12.63	12.61	0.073	0.110	0.126
#3	36.6	28.36	8.36	12.63	12.61	0.073	0.145	0.244

Table 4-6, the stiffness tensors (GPa) and Thomsen parameters of three models.

For the first model, the vertical slowness versus horizontal one is plotted in figure 4-7-1. It can be seen that the behavior of the simplified qP-wave slowness is close to the full

solution. However the qSV-wave is deviant from the exact one at large horizontal slowness. Tsvankin and Thomsen (1994) have pointed out that qSV-wave's velocity behavior is determined by the parameter σ (equation 4-4) which is directly related with “ $\delta - \varepsilon$ ”. I receive the same conclusion that this parameter will also influence the slowness behavior since it appears explicitly in equation 3-15-b. The deviant of the approximated slowness is resulted from the high σ value. This will lead to the significant error in SPP calculation and eventually to the big error in qSV-wave radiation pattern (figure 4-7-2 and 4-7-3).

$$\sigma = \frac{C_{33}}{C_{44}}(\varepsilon - \delta) = \frac{\delta - \varepsilon}{f - 1} \quad (4-4)$$

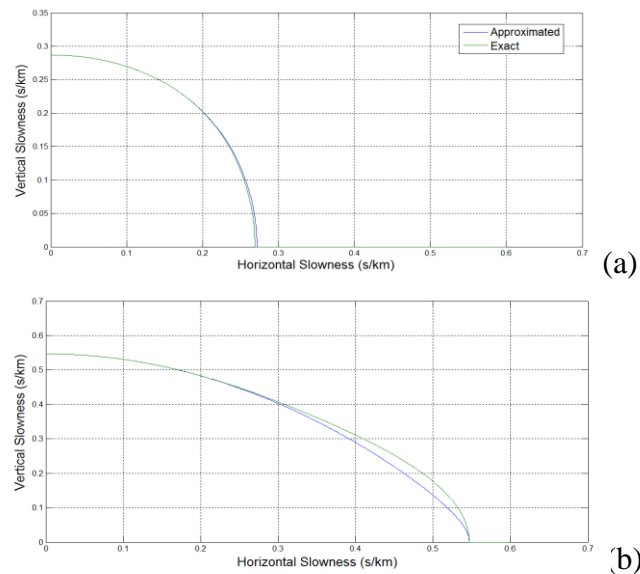


Figure 4-7-1, Approximated and exact qP- (a) and qSV-wave (b) vertical slowness behavior versus horizontal slowness for model one.

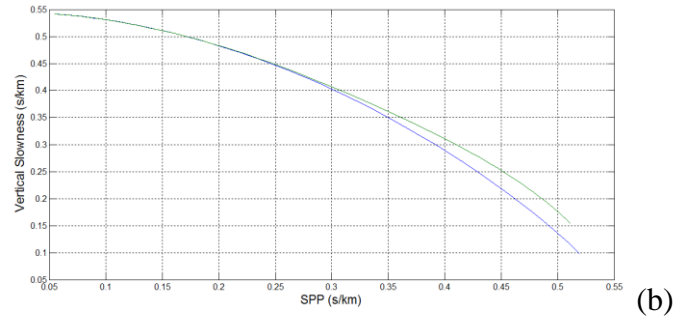
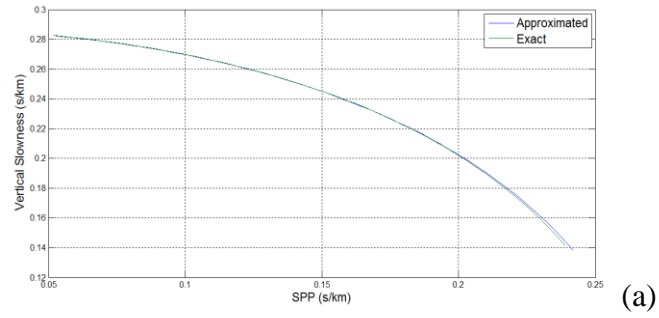


Figure 4-7-2, qP- (a) and qSV-wave (b) SPP calculation for model one.

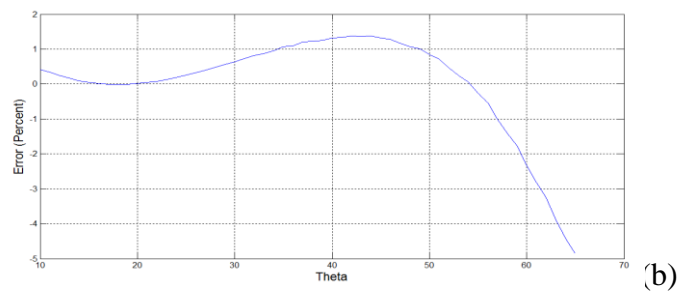
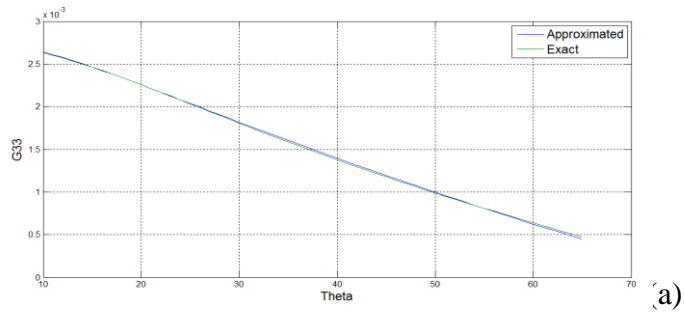


Figure 4-7-3, qP-wave far-field radiation patterns of G_{33} (a) for model one and its relative error (b).

The radiation patterns of the media in equation 4-3 and their relative error is plotted in figures 4-7-1 to 4-7-8 for G_{33} , G_{11} , and G_{13} , respectively. The errors are calculated by equation 4-5. For the qP-wave, the approximated solution behaves very well. The error is lower than 1.5% for the most cases. However, the qSV-wave behaves well at small polar angles (less than 30 degree) and the error increase rapidly around 50 to 60 degrees. The exact radiation changes more rapidly at 45 degree but the approximated one changes more smoothly.

$$o = \frac{G_{apx} - G_{ext}}{G_{ext}} \quad (4-5)$$

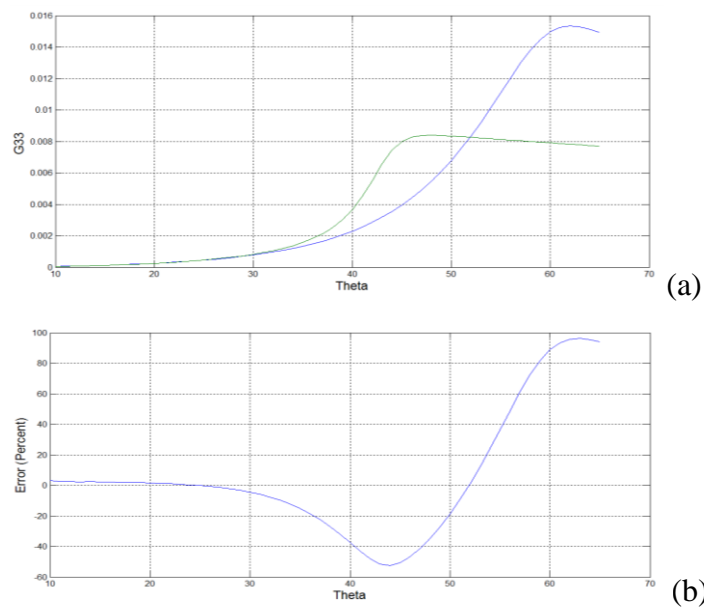


Figure 4-7-4, qSV-wave far-field radiation patterns of G_{33} (a) for model one and its relative error (b).

The behavior of G_{11} and G_{13} is not far from G_{33} . For the qP-wave, the error will grow as the polar angle increase. The qSV-wave radiation behaves better than the G_{33} . Similarly, the full solution is more angular than the approximated one. It is because the second-order simplified dispersion relationship can only be a smooth approximation of the exact solution and are unable to model the rapid change of radiation pattern.

The difference in the error trends is caused by the different structure of the Green's tensor. The hybrid method which using the numerical method to find the SPP and substitute them into Green's tensor may help to lower the error at intermediate polar angles, but cannot lower the highest error significantly.

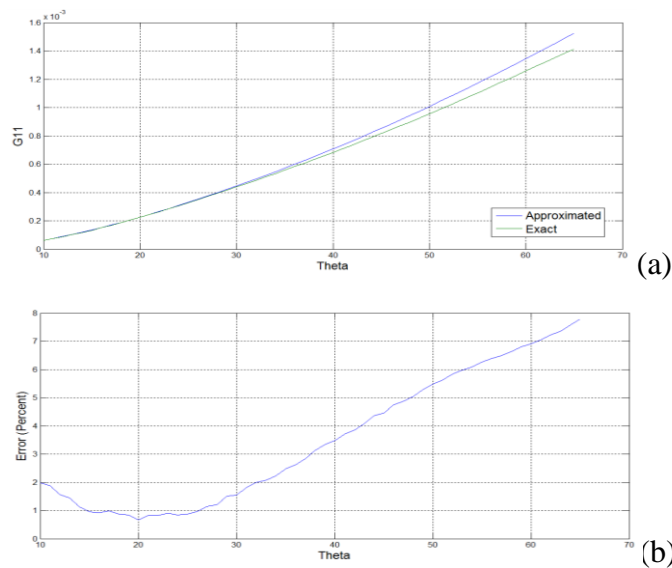


Figure 4-7-5, qP-wave far-field radiation patterns of G_{11} (a) for model one
its relative error (b).

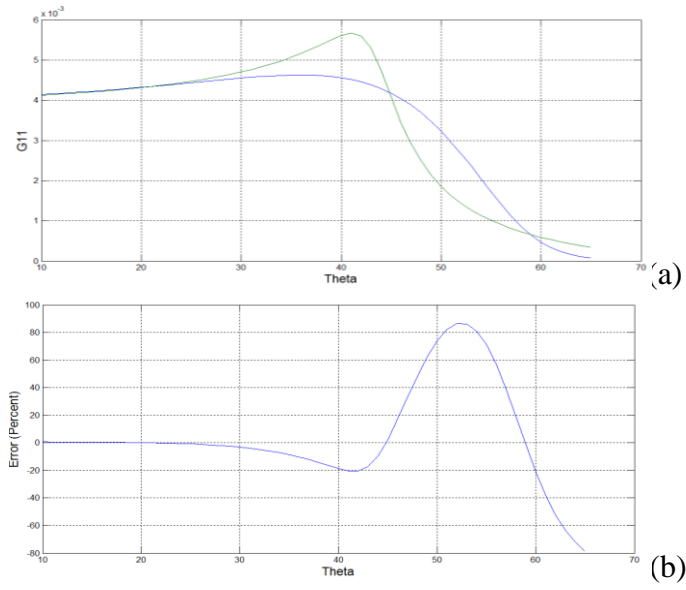


Figure 4-7-6, qSV-wave far-field radiation patterns of G_{11} (a) for model one and its relative error (b).

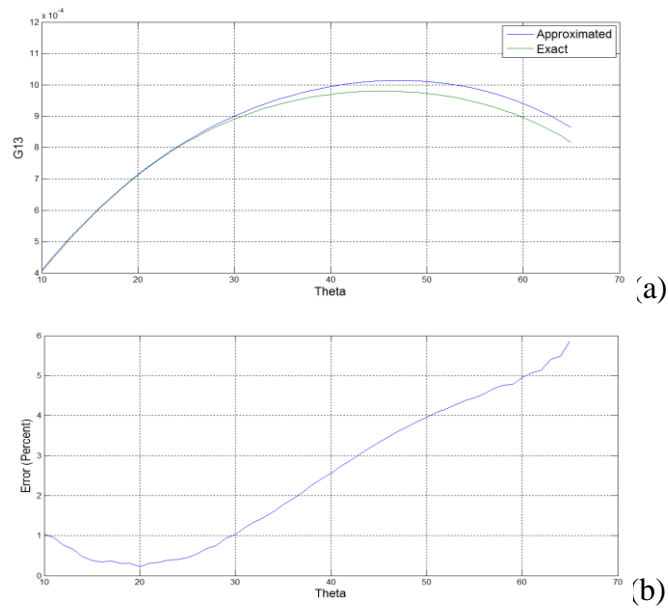


Figure 4-7-7, qP-wave far-field radiation patterns of G_{13} (a) for model one and its relative error (b).

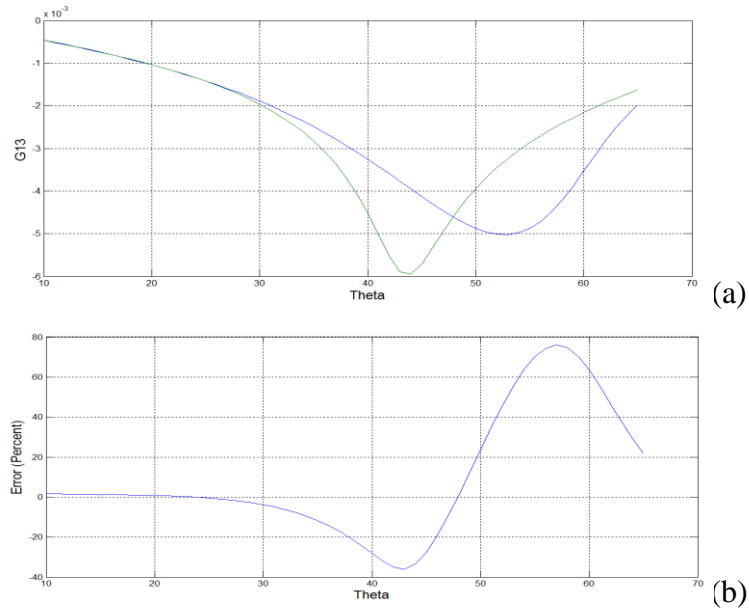


Figure 4-7-8, qSV-wave far-field radiation patterns of G_{13} (a) for model one and its relative error (b).

The results of model two are shown in figures 4-8-1 to 4-8-7 in the same manner of model one. Figure 4-8-1-a and 4-8-1-b are the calculation of SPPs for qP- and qSV-wave. Figure 4-8-1-b shows the approximated slowness of qSV-wave is much closer than model one due to the lower value of σ . The approximated radiation patterns are also closer to the exact ones for the same reason.

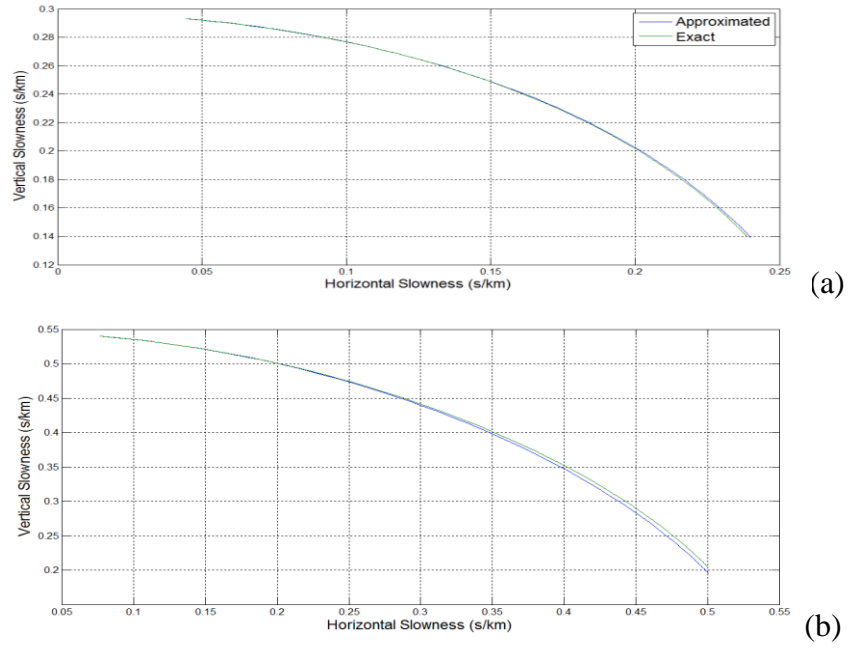


Figure 4-8-1, Calculated SPP for qP- and qSV-wave for model two.

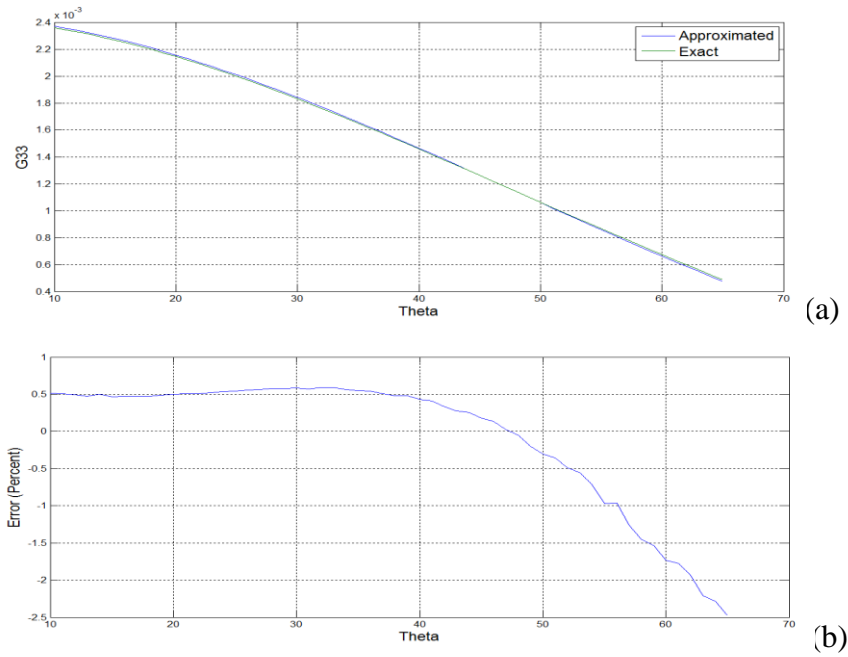


Figure 4-8-2, qP-wave far-field radiation patterns of G_{33} (a)

for model two and its relative error (b).

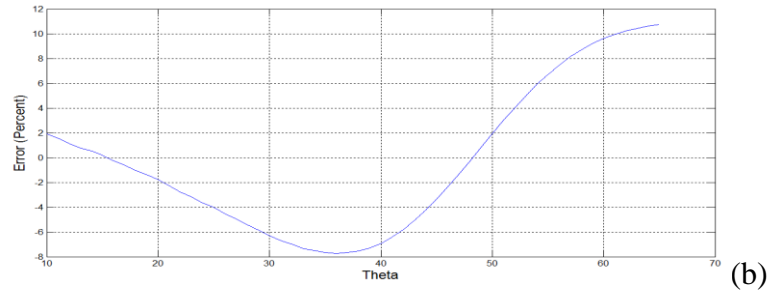
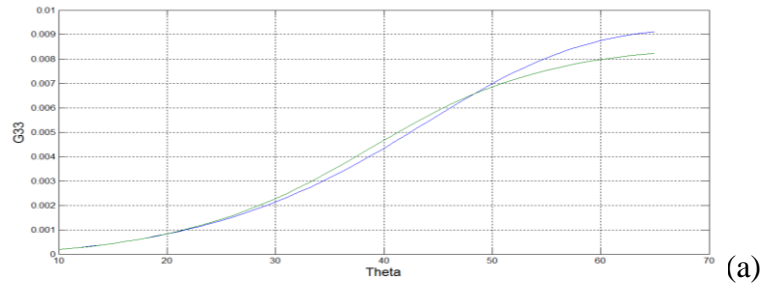


Figure 4-8-3, qSV-wave far-field radiation patterns of G_{33} (a)
for model two and its relative error (b).

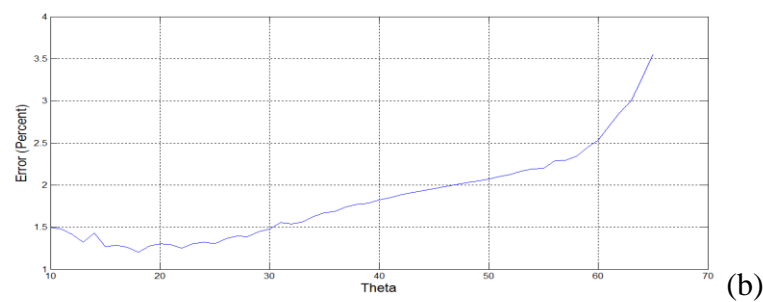
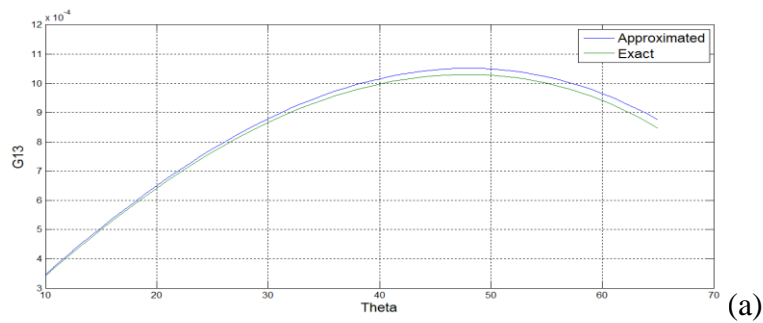


Figure 4-8-4, qP-wave far-field radiation patterns of G_{13} (a)
for model two and its relative error (b).

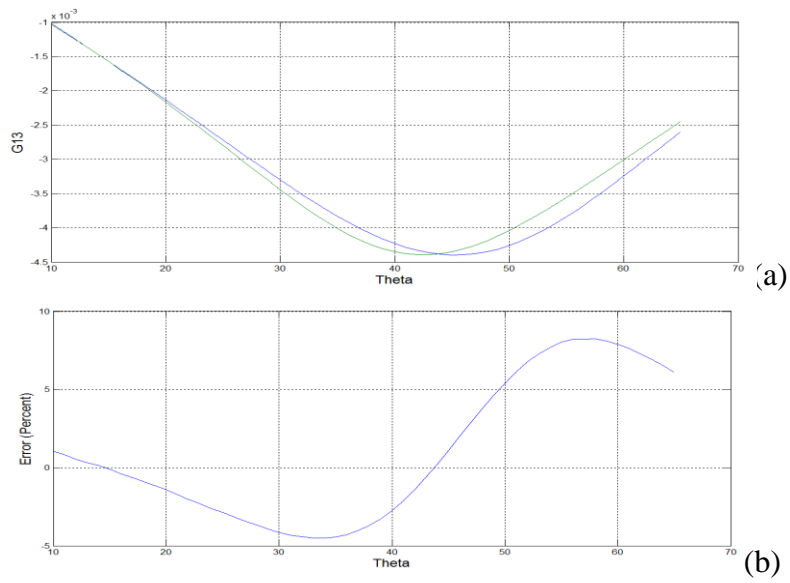


Figure 4-8-5, qSV-wave far-field radiation patterns of G_{13} (a) for model two and its relative error (b).

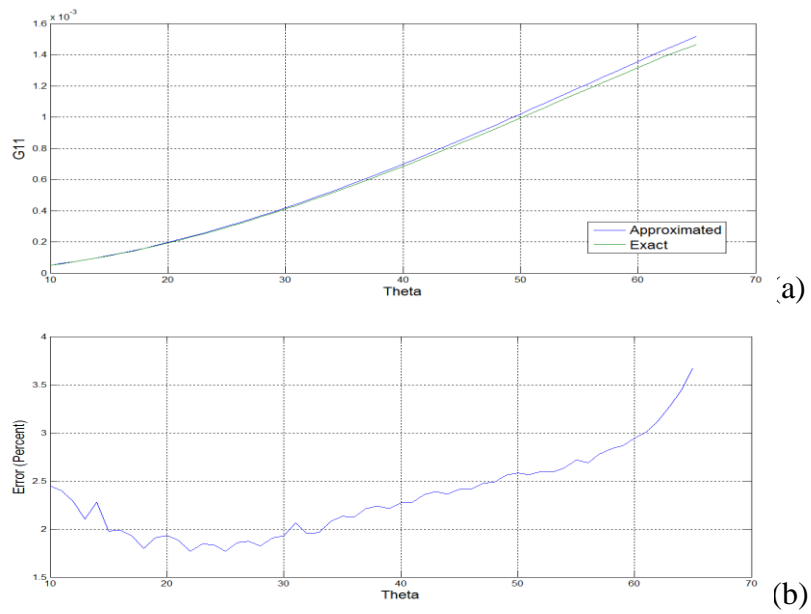


Figure 4-8-6, qP-wave far-field radiation patterns of G_{11} (a) for model two and its relative error (b).

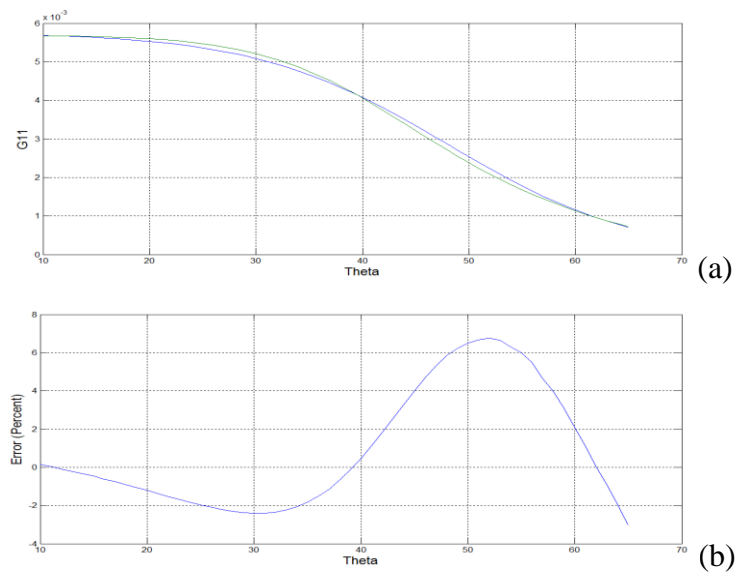


Figure 4-8-7, qSV-wave far-field radiation patterns of G_{11} (a) for model two and its relative error (b).

The results for model three are plotted in figures 4-9-1 to 4-9-7. Thomsen parameters ϵ and δ are higher than those from model two. There is a larger deviant of both the qP and qSV slowness. This will lead to a bigger error in the radiation patterns.

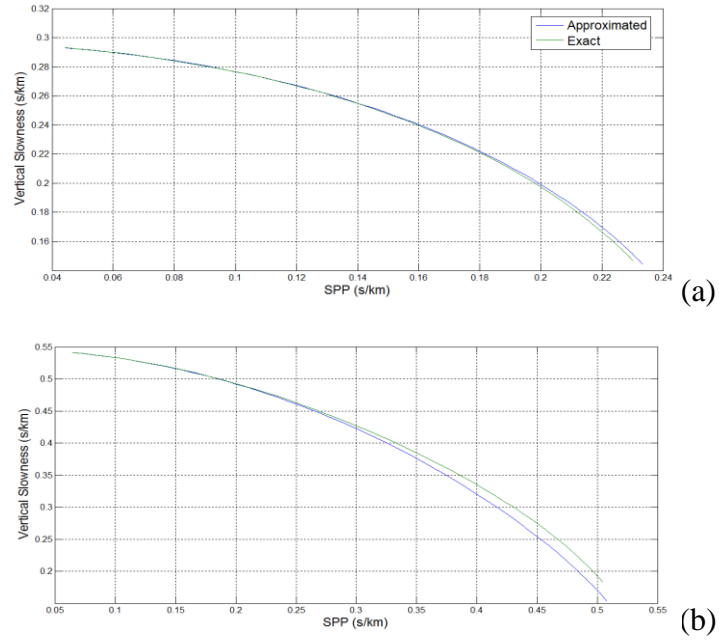


Figure 4-9-1, Calculated SPP for qP- and qSV-wave for model three.

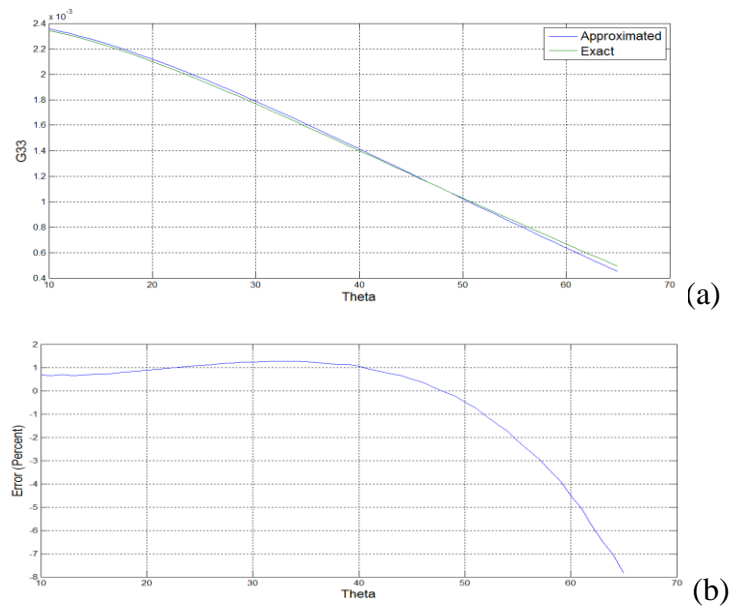


Figure 4-9-2, qP-wave far-field radiation patterns of G_{33} (a)

for model three and its relative error (b).

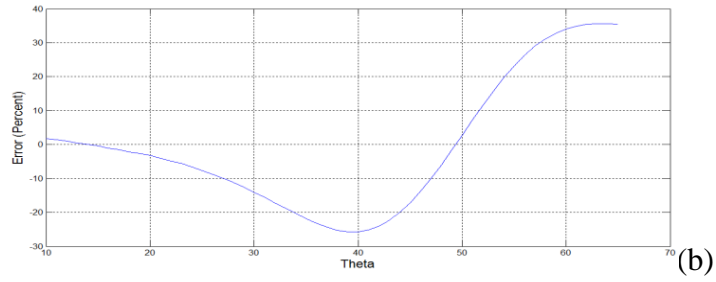
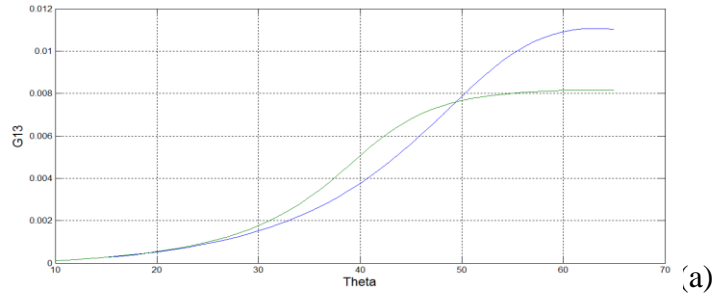


Figure 4-9-3, qSV-wave far-field radiation patterns of G_{33} (a)
for model three and its relative error (b).

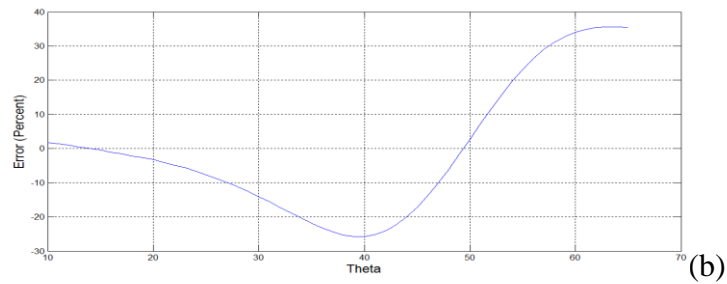
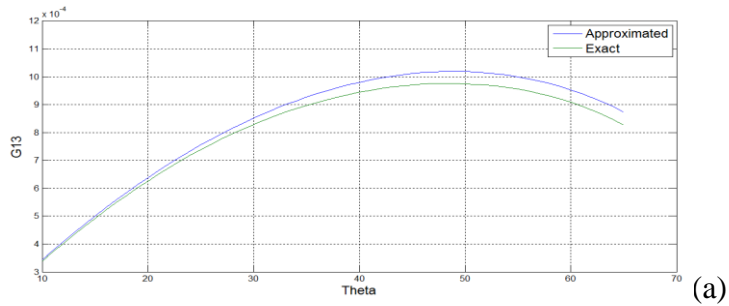


Figure 4-9-4, qP-wave far-field radiation patterns of G_{13} (a)
for model three and its relative error (b).

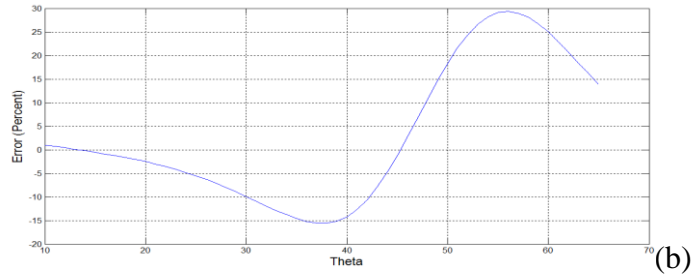
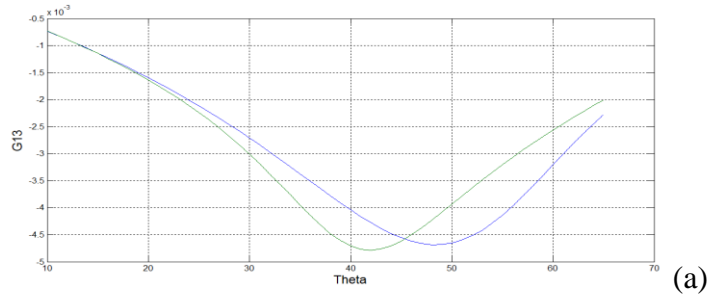


Figure 4-9-5, qSV-wave far-field radiation patterns of G_{13} (a)
for model three and its relative error (b).

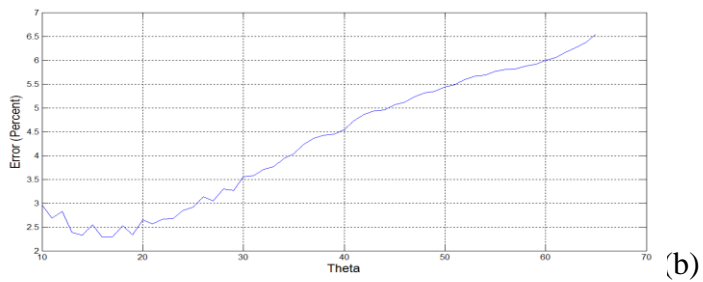
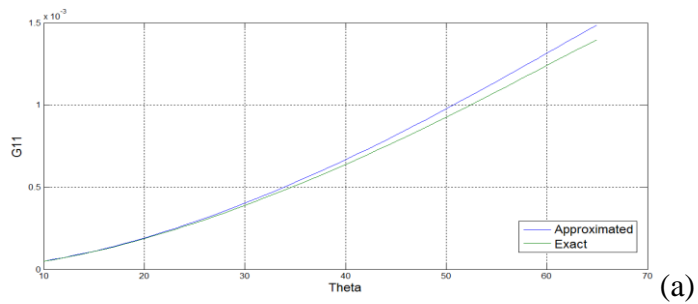


Figure 4-9-6, qP-wave far-field radiation patterns of G_{11} (a)
for model three and its relative error (b).

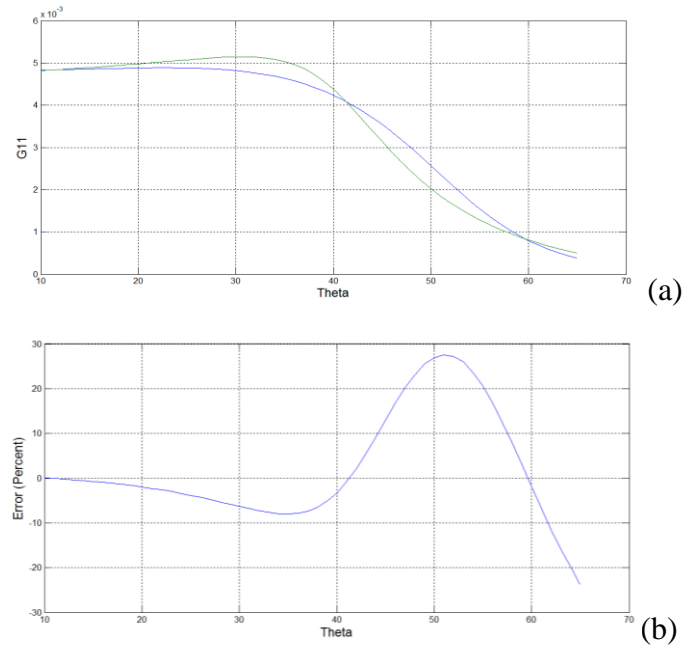


Figure 4-9-7, qSV-wave far-field radiation patterns of G_{11} (a) for model three and its relative error (b).

4.2 Synthetic seismograms in the homogeneous media

In this section, the synthetic seismograms are shown and studied. First, the theory is quickly reviewed. Then, the analytical far-field seismograms and the numerically calculated full-waveform solutions are shown in the second section.

4.2.1 Introduction

Recalling equation 1-2, the displacement is the superposition of the elementary solutions (Green's tensor). In this section, I only consider the homogeneous medium. And I am focusing on study the individual part of the Green's tensor.

The calculated radiation patterns are indicating the amplitude variation over different directions. The time arrival is depended on the accuracy of the stationary slowness. For the approximated results, the approximated slowness of both qP- and qSV-wave are already studied in the above section.

The full-wave-form exact solution can be found by calculating the integral over horizontal slowness numerically. There is a singularity at the interface between the real and complex vertical slowness. Generally, it will not contribute to the result and can be removed by simple methods (Tsvankin and Chesnokov, 1990).

4.2.2 Synthetic examples

In this section, three models are studied. All the parameters are listed in Table 4-10. The first model is the elliptical anisotropic medium in equation 4-2. The second one is the weak TI medium in the previous section. The last model is a VTI medium with strong anisotropic properties which will lead to shear wave triplication. For the first two models, both the analytical and numerical results are studied. For the third one, only the numerical results are shown.

Model	C_{11}	C_{33}	C_{44}	C_{66}	C_{13}	P
#1	3.52	2.02	0.31	0.42	2.03	1.8

#2	34.60	28.36	8.36	12.63	12.61	2.5
#3	19.38	12.05	3.00	5.43	5.22	2.5

Table 4-10, stiffness tensor (GPa) and density (g/cc) for three different models.

The results for model one are plotted in figures 4-11-1 to 4-11-3 and 4-11-4 to 4-11-6. The source is located at the origin and there are three receivers located at different offsets (X=Y=0.5 km, X=Y=0.8 km, and X=Y=1.1 km). For those in figures 4-11-1 to 4-11-3, the force is along the Z-axis and I calculate its contribution to vertical (G_{33}) and horizontal (G_{13}) displacements. Figures 4-11-4 to 4-11-6 show the results of X-component receivers due to forces along the X-axis. The wavelet being used for numerical calculation is described in equation 4-6. The analytical solutions are plotted with the same magnitude but only with the Dirac delta function.

$$f(t) = Ae^{-bt}$$

$$A = 40000 \text{ N} \quad (4-6)$$

$$b = 90 \text{ 1/s}$$

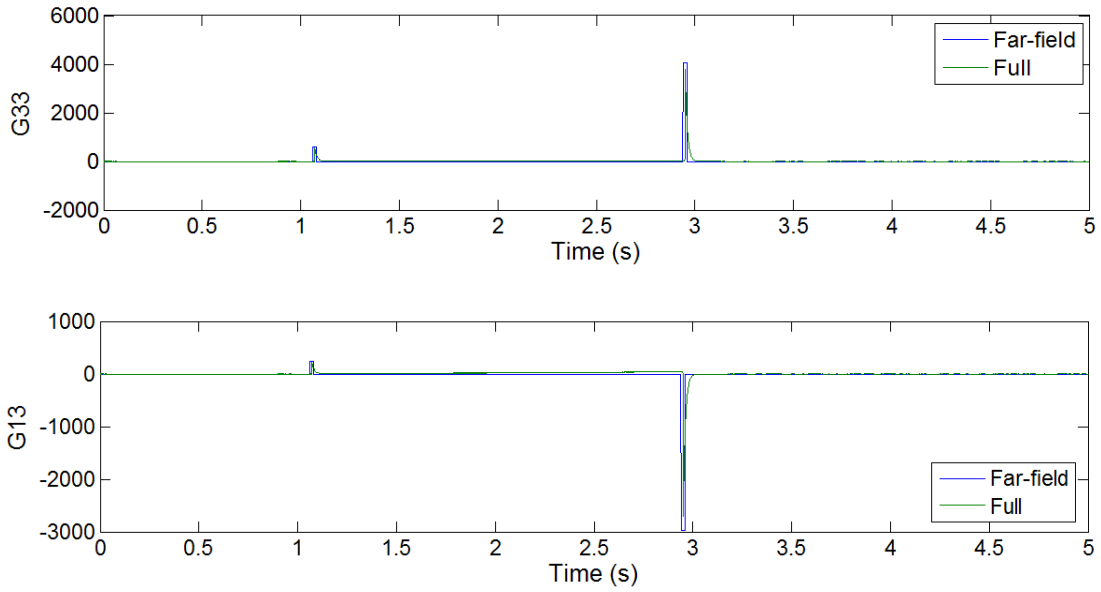


Figure 4-11-1, Z and X components at X=Y=0.5 Z=1 from Z source for model one.

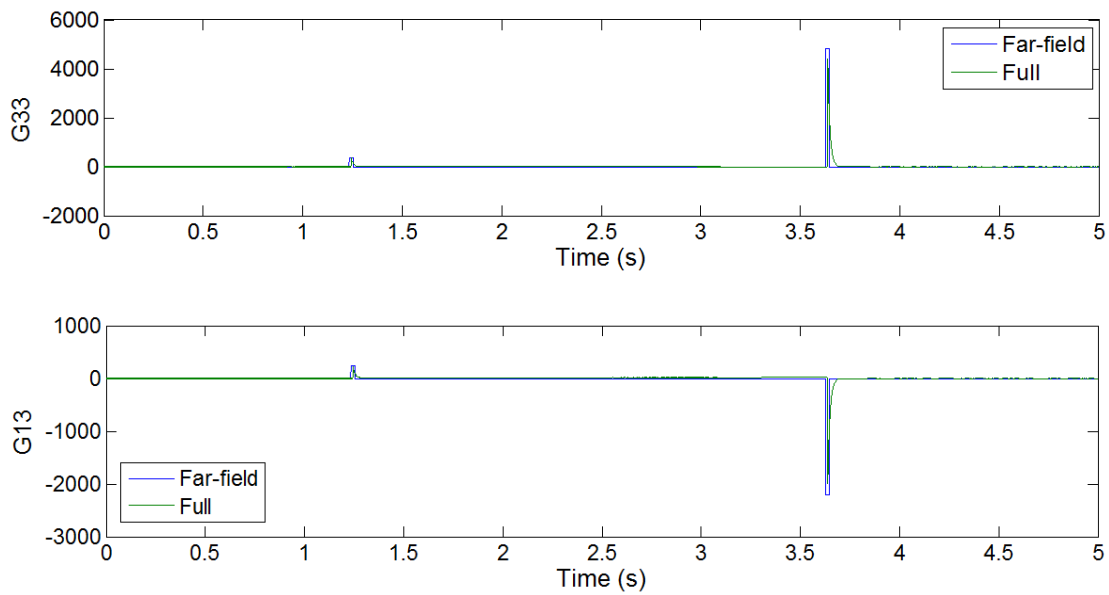


Figure 4-11-2, Z and X components at X=Y=0.8 Z=1 from Z source for model one.

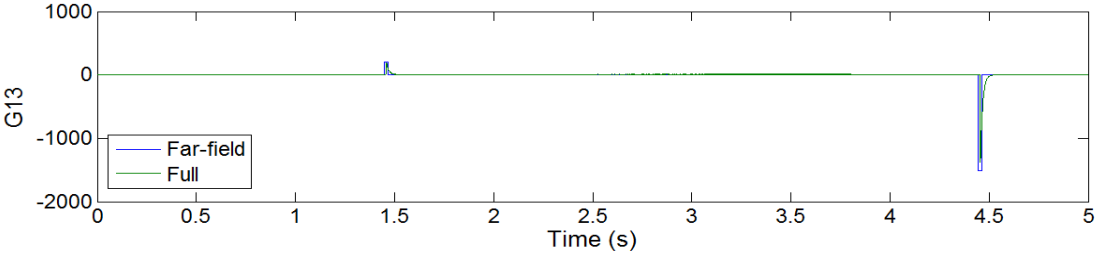
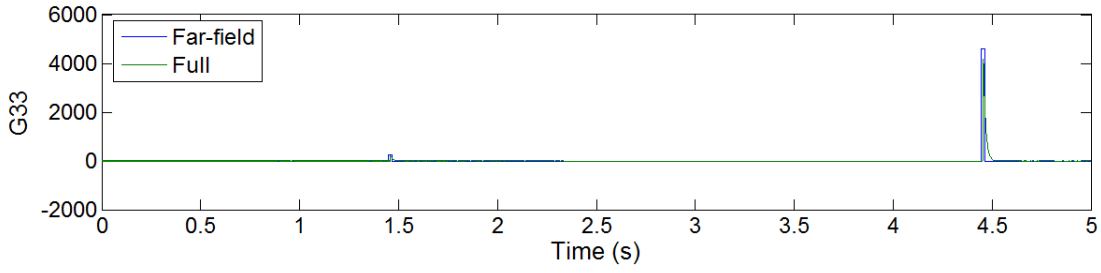


Figure 4-11-3, Z and X components at X=Y=1.1 Z=1 from Z source for model one.

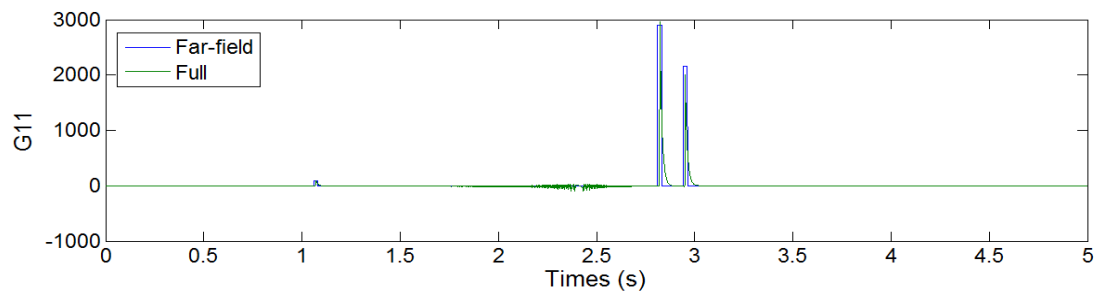


Figure 4-11-4, X component at X=Y=0.5 Z=1 from X source for model one.

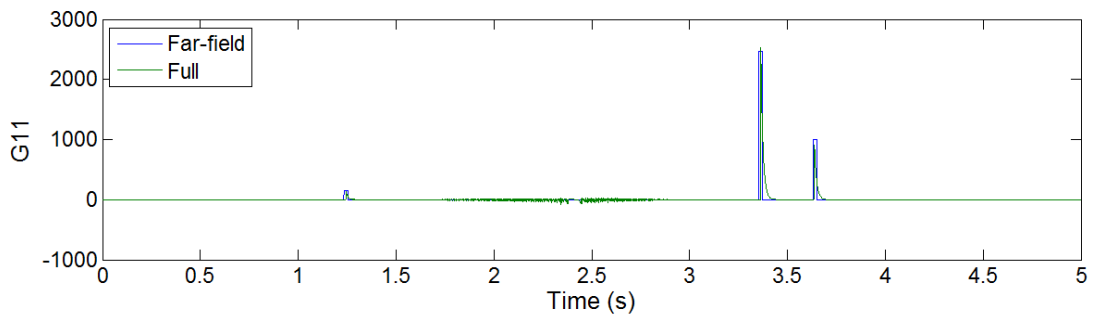


Figure 4-11-5, X component at X=Y=0.8 Z=1 from X source for model one.

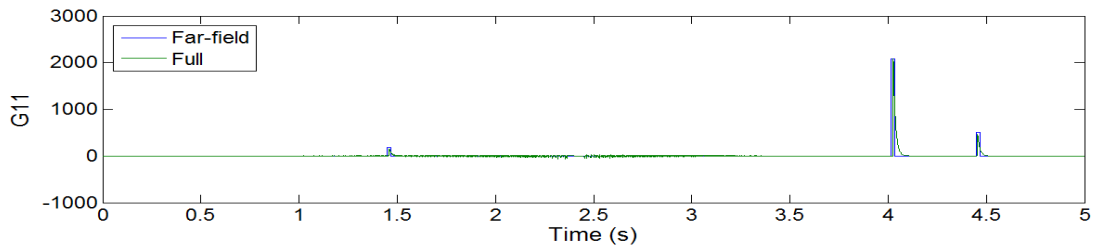


Figure 4-11-6, X component at $X=Y=1.1$ $Z=1$ from X source for model one.

The results for model two are plotted in figures 4-12-1 to 4-12-6 by the same manner. The location of receivers was different ($X=Y=1$ km, $X=Y=1.5$ km, and $X=Y=2$ km). It can be seen that the approximated qP and qSV solutions are following the behavior of radiation patterns described in the previous section (figures 4-8-2 to 4-8-7).

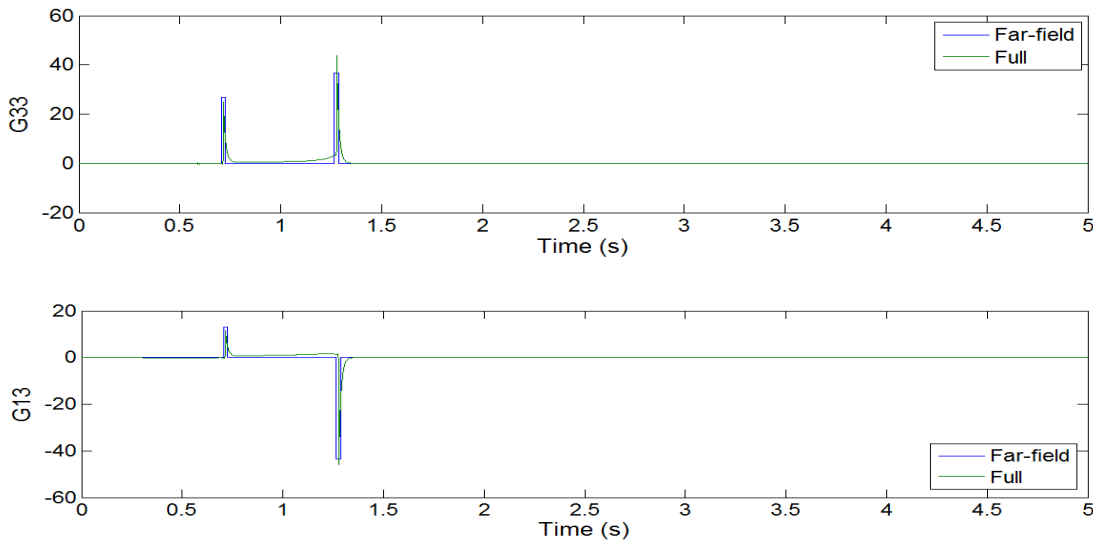


Figure 4-12-1, Z and X components at $X=Y=1$ $Z=2$ from Z source for model two.

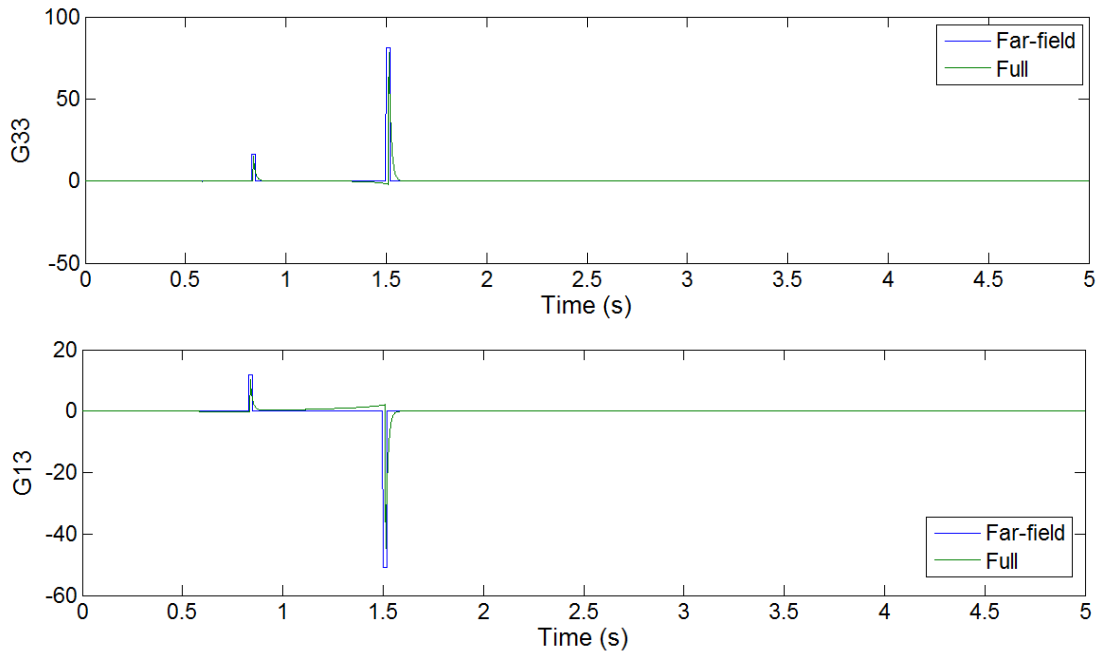


Figure 4-12-2, Z and X components at X=Y=1.5 Z=2 from Z source for model two.

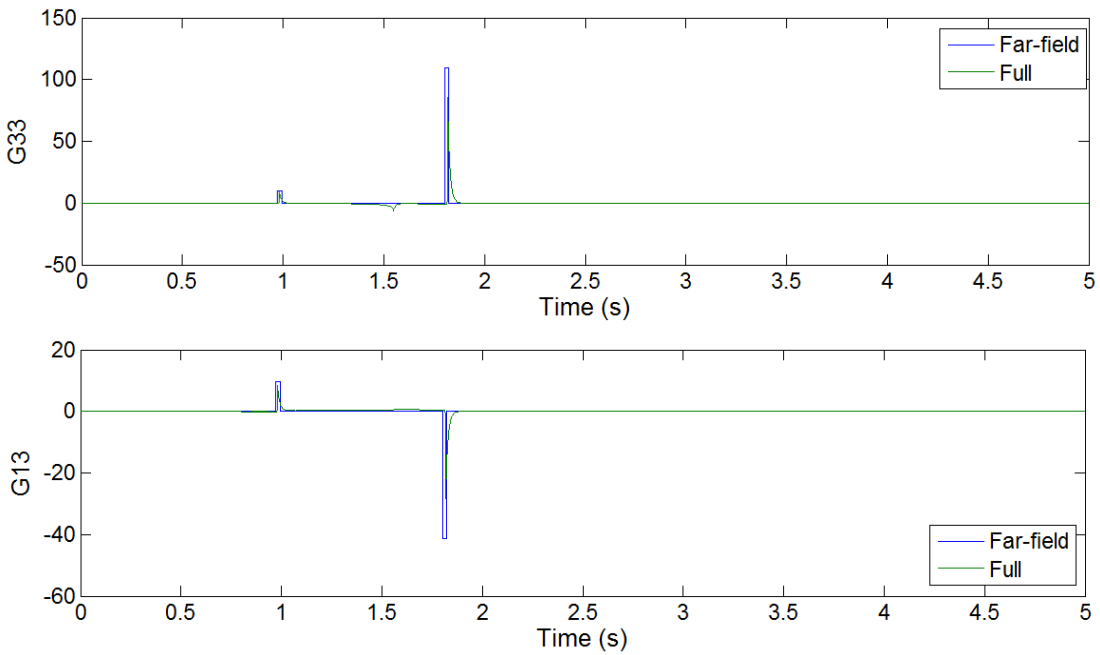


Figure 4-12-3, Z and X components at X=Y=2 Z=2 from Z source for model two.

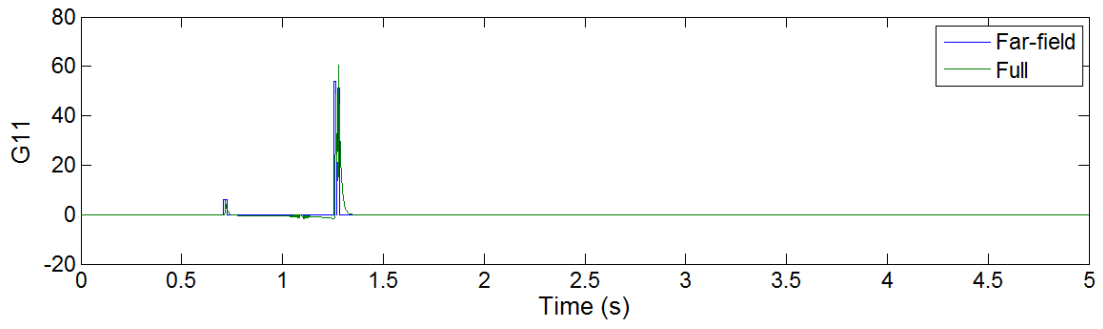


Figure 4-12-4, X component receiver at X=Y=1 Z=2 from X source for model two.

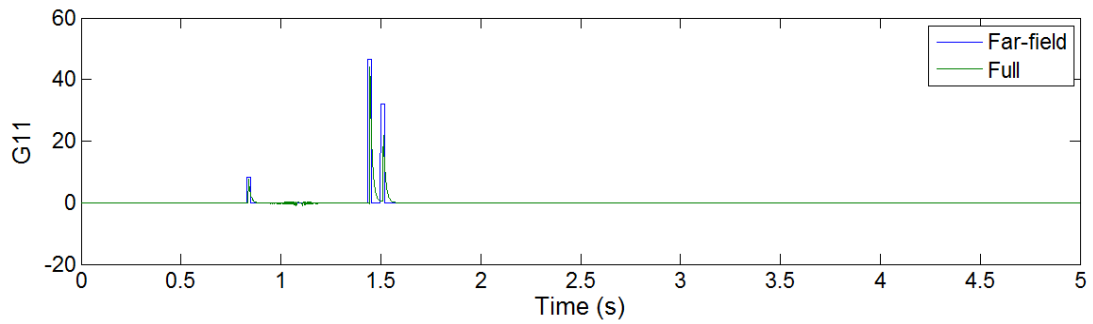


Figure 4-12-5, X component at X=Y=1.5 Z=2 from X source for model.

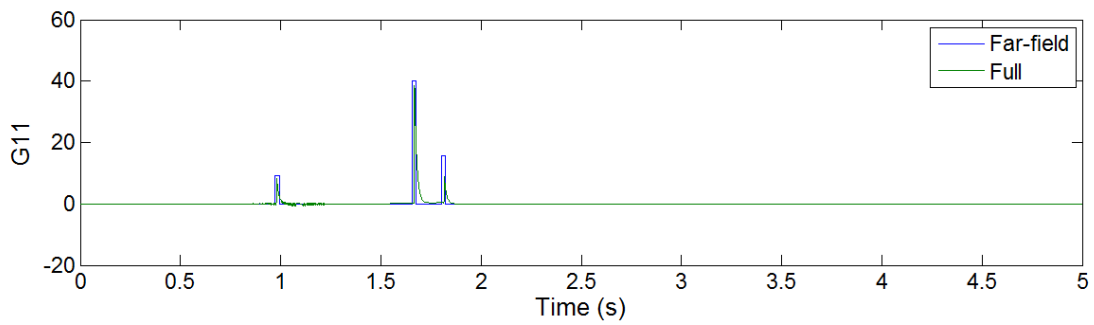


Figure 4-12-6, X component at X=Y=2 Z=2 from X source for model.

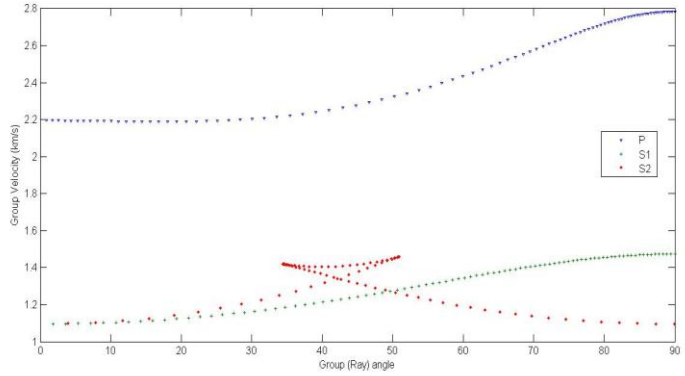


Figure 4-13, Group velocities for qP, qSV, and SH in model three.

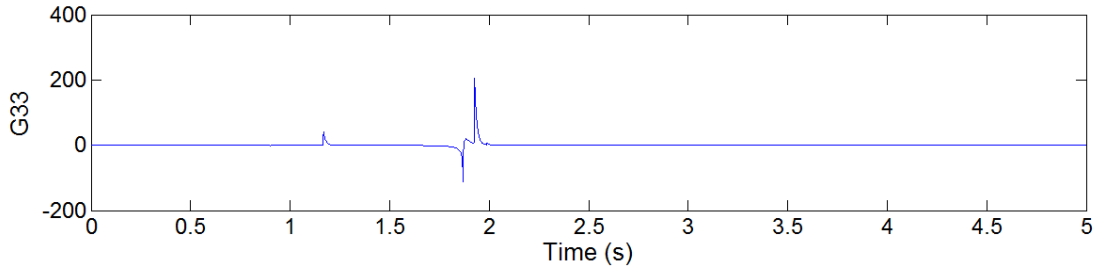


Figure 4-14-1, Z component at X=Y=1.2 Z=2 from Z source for model three.

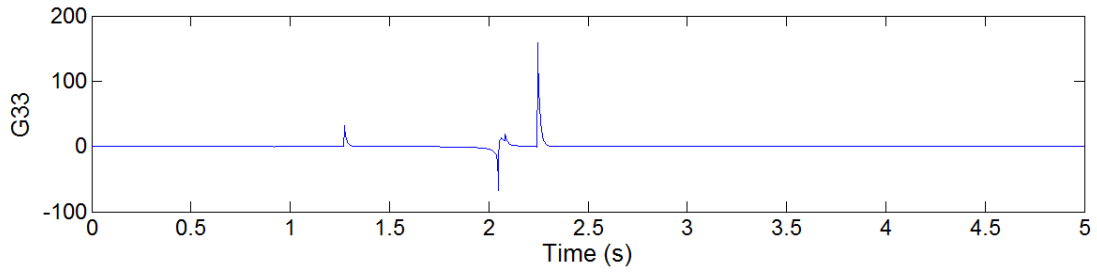


Figure 4-14-2, Z component at X=Y=1.5 Z=2 from Z source for model three.

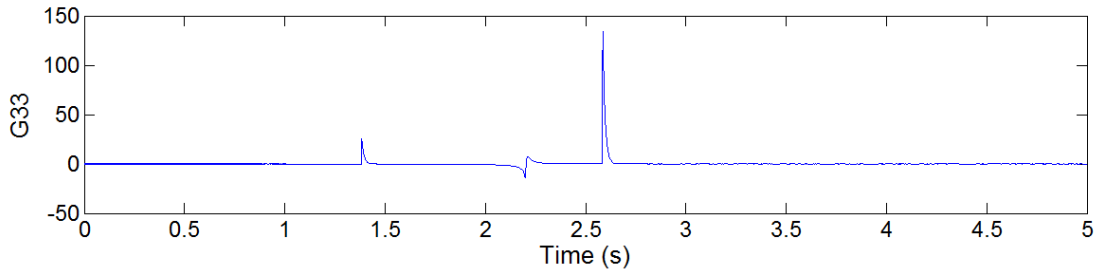


Figure 4-14-3, Z component at $X=Y=1.8$ $Z=2$ from a Z source for model three

The group velocity for model three is calculated and plotted in figure 4-13. The corresponding seismograms are plotted in figures 4-14-1 to 4-14-3 for G_{33} . There are additional qS-wave travel between the usual qP- and qSV-wave.

This effect can be modeled by the numerical calculation. The energy participation in this case is very complicated. The wave-front is strongly tilted and the solutions are accompanied with the phase shift. The simple stationary phase approximation is not accurate for this type of phenomenon.

5 Conclusion of Part I

New forms of elastodynamic Green's tensor in VTI medium are founded based on Tsvankin and Chesnokov's method (1990).

The asymptotic solution of elastodynamic Green's tensor is calculated analytically for the elliptical anisotropic medium. The approximated far-field qP-qSV solution for the weak VTI medium is found by expanding the slowness into small Thomsen parameters based on a newly proposed method. The asymptotic SH-wave, which is essentially elliptical, can always be calculated analytically.

The solution of elliptical anisotropy is exact and agrees very well with the results obtained by other methods (Gajewski, 1993). For the weak VTI medium, the accuracy of the solution is depending on the value of Thomsen parameters. The accuracy of the qP and qSV-wave are related with the parameters δ and ϵ . For the qSV-wave, the situation is more complicated. The parameter σ is determining its behavior. When this parameter is big enough, the qSV-wave front will be strongly twisted. At this time, this method fails to work and the numerical solution is suggested.

Generally speaking, the solution of qP-wave is more accurate than the qSV-wave. The accuracy of both of them will decrease toward the horizontal plane.

Part II

Green's tensor in pre-stressed medium

In this part, the effects of static initial stress on the elastic wave propagation are studied. At first, the theory of Nikitin and Chesnokov (1981) is introduced and the method of calculating the elastodynamic Green's tensor is briefly reviewed. Then the behavior of the phase velocity under initial stress is studied. In the last section, four models of initial stress were studied and the results are discussed.

The intuitive understanding of the influence of initial stress on elastic wave propagation can be simply illustrated by the following 1-D rope example, which is mentioned in Biot's paper (1940). Considering the rope, whose elastic property can be described by the Young's modulus, being stretched or relaxed. Its elastic property will be changed. And if there is an elastic wave propagates through, it will travel faster in the stretched rope than the relaxed one.

The effect of stress will have a similar impact on the background medium. Combining the compacting (or relaxing) with its six-independent elements, the stress tensor may result in different symmetry to those caused by other geological reason.

The thought experiment can be described by the following steps:

At first, the background medium is presented, which is isotropic and without any cracks

or defects.

Secondly, the initial stress is applied to the medium. At this time, the symmetry of the medium may be altered. The symmetry can be complicated due to the structure of the deviatoric stress.

Lastly, the point source was triggered and the elastodynamic Green's tensor is calculated.

6 The setting of the problem

6.1 Wave equation in pre-stressed medium

The displacement u_i is defined as the difference between the present coordinate (Eulerian variable) x_i and the original coordinate (Lagrangian variable) a_i .

$$u_i = x_i - a_i$$

The stress σ_{ij} in the present coordinate system can be written as the rotation of the stress in original coordinate system τ_{ij} which is also known as the second Piola-Kirchhoff stress tensor (equation 6-1).

$$\sigma_{ij} = J(x, a) \frac{\partial x_i}{\partial a_k} \frac{\partial x_j}{\partial a_l} \tau_{kl} \quad (6-1)$$

$J(x, a)$ is the Jacobian. It links the densities in present (ρ) and the original coordinate system (ρ_0). (Bland, 1969)

$$J(x, a) = \frac{\rho}{\rho_0}$$

$$\rho(\mathbf{r}, t) \frac{\partial^2 u_i(\mathbf{r}, t)}{\partial t^2} = \frac{\partial \sigma_{ij}(\mathbf{r}, t)}{\partial x_j} + f_i(\mathbf{r}, t) \quad (6-2)$$

The elastic wave equation in general anisotropic media can be written as equation 6-2. f_i is the force density which has the unit of force over volume. Take equation 6-1 into 6-2 and considering the equilibrium initial stress, equation 6-3 is obtained.

$$\rho_0 \frac{\partial^2 u_i}{\partial t^2} = \left(\frac{\partial \tau_{jl}}{\partial a_l} \frac{\partial u_i}{\partial a_j} + \tau_{jl} \frac{\partial^2 u_i}{\partial a_l \partial a_j} + \frac{\partial \tau_{ij}}{\partial a_j} \right) + f_i \quad (6-3)$$

The stress in the original coordinate can be written as the summation of the initial static stress τ_{ij}^0 and the stress excited by the elastic wave propagation σ_{ij}^* , which is equation 6-4-1. The initial static stress can be presented in terms of the initial pressure P_0 and deviatoric stress τ_{ij}^0 (6-4-2). The negative sign in front of the pressure is chose to make positive

pressure is to relax the medium. Equation 6-5 is the Hooke's law for the second Piola-Kirchhoff stress.

$$\tau_{ij} = \tau_{ij}^0 + \sigma_{ij}^* \quad (6-4-1)$$

$$\tau_{ij}^0 = -P_0 \delta_{ij} + t_{ij}^0 \quad (6-4-2)$$

$$\sigma_{ij}^* = T_{ijkl} \frac{\partial u_k}{\partial x_l} \quad (6-5)$$

The stiffness tensor in pre-stressed media can be found by expanding the strain energy into Taylor series of the deviatoric initial stress (Nikitin and Chesnokov, 1981). In general it can be presented by equation 6-6. The first term is the stiffness tensor of the background medium under pressure and the second term is corresponded to initial deviatoric stress.

There are two conditions in Nikitin and Chesnokov's theory (1981). First, the initial static stress is small compared to the stiffness tensor of the background medium. Secondly, the background medium is without any inclusion or fractures.

$$T_{ijkl}(\tau_{mn}^0) = C_{ijkl}^0(P_0) + B_{ijklmn}(P_0)t_{mn}^0 \quad (6-6)$$

$$\begin{aligned} T_{ijkl} = & \lambda(P_0)\delta_{ij}\delta_{kl} + \mu(P_0)(\delta_{il}\delta_{kj} + \delta_{ik}\delta_{jl}) + \nu_1(P_0)(t_{ij}^0\delta_{kl} + \delta_{ij}t_{kl}^0) \\ & + \frac{\nu_2(P_0)}{2}(t_{il}^0\delta_{jk} + \delta_{jl}t_{ik}^0 + \delta_{il}t_{jk}^0 + \delta_{ik}t_{jl}^0) \end{aligned} \quad (6-7)$$

If the background media is isotropic, equation 6-6 becomes equation 6-7. In equation 6-7, δ_{ij} is Kronecker symbol, while λ and μ are Lamé parameters. v_1 and v_2 are the dimensionless parameters in matrix B_{ijklmn} . All of them are depended on the initial pressure. The pressure dependency is not limited to the linear relationship. It will not affect the symmetry but the strength of the medium.

Incorporating equation 6-4 and 6-5 into equation 6-3 then removing the higher-order terms, the elastic wave equation in original coordinate system can be found.

$$\rho_0 \frac{\partial^2 u_i}{\partial t^2} = \left(\frac{\partial \tau_{jl}^0}{\partial a_l} \frac{\partial u_i}{\partial a_j} + \tau_{jl}^0 \frac{\partial^2 u_i}{\partial a_l \partial a_j} + \frac{\partial}{\partial a_j} T_{ijkl} \frac{\partial u_k}{\partial a_l} \right) + f_i \quad (6-8)$$

For the homogeneously distributed initial stress, equation 6-8 becomes equation 6-9. It is important to notice that the first term on the right-hand side will vanish when the initial stress is zero. Then equation 6-9 is similar to the Eulerian wave equation.

$$\rho_0 \frac{\partial^2 u_i}{\partial t^2} = \tau_{jl}^0 \frac{\partial^2 u_i}{\partial a_l \partial a_j} + T_{ijkl} \frac{\partial^2 u_k}{\partial a_l \partial a_j} + f_i \quad (6-9)$$

Equation 6-10 is the equation for Green's tensor. The displacement can be written as the superposition of the elementary solution (equation 6-11). I will solve equation 6-10 to find the radiation patterns.

$$(\rho_0 \delta_{ik} \frac{\partial^2}{\partial t^2} - \tau_{jl}^0 \delta_{ik} \frac{\partial^2}{\partial a_l \partial a_j} - T_{ijkl} \frac{\partial^2}{\partial a_j \partial a_l}) G_{km} = \delta_{im} \delta(\mathbf{r} - \mathbf{r}_0) \delta(t - t_0) \quad (6-10)$$

$$u_k(\mathbf{r}, t) = G_{km} * f_m = \iint G_{km}(\mathbf{r}, t; \mathbf{r}_0, t_0) f_m(\mathbf{r}_0, t_0) d\mathbf{r}_0 dt_0 \quad (6-11)$$

The Green's tensor in wave-number–frequency-domain (bilinear form of Green's tensor) can be easily founded (equation 6-12).

$$G_{ij}(\mathbf{k}, \omega) = \sum_{\eta=p,sv,sh} \frac{l_i^\eta l_j^\eta}{\rho_0 (k^2 V_\eta^2 - \omega^2)} \quad (6-12)$$

η indicates the mode of elastic wave (qP, qSv, or qSH). Equation 6-12 can be interpreted as the summation of the contribution of different modes denoted by η . l_i^η is the eigenvectors in for each mode. ω is the angular frequency and k is the wave number. V_η is the phase velocities which can be anisotropic.

6.2 Calculation of the Green's tensor

Tsvankin and Chesnokov (1990) proposed a method to calculate the far-field part of the radiation patterns in general elastic media. It's based on finding the Green's tensor in frequency – slowness (or wave-vector) domain (equation 6-12) and find its Fourier image in time-space domain. This method involved solving the four-dimensional integral of inverse

Fourier transform (3-D in space and 1-D in time).

The cylindrical coordinate system is chose to do the computation and the integral formula can be written as equation 6-13.

$$G_{ij}(r, z, \alpha, t) = \frac{1}{(2\pi)^4} \int_{-\infty}^{\infty} \int_0^{2\pi} \int_{-\infty}^{\infty} \int_0^{\infty} G_{ij}(k_r, k_3, \varphi, \omega) e^{-i[k_r r \cos(\varphi - \alpha) + k_3 z]} e^{i\omega t} k_r dk_r dk_3 d\varphi d\omega$$

(6-13)

The first integral over vertical wave-number k_3 can be solved by residue theorem.

The second integral over azimuth angle φ can be solved by expanding the integrand into low order Fourier series (equation 6-14) and the integral may be reduced by Bessel integrals.

This step is omitted in the previous sections because that the azimuthally dependent property of the Green's tensor in VTI medium is only to the second order of the Fourier series. For the case of initial stress, the integrand is the Green's tensor which has two variables – polar angle (θ) and azimuth angle (φ). The Green's tensor is expanded into the low-order Fourier series of azimuth angle. The vertical slowness is expanded to the first-order Fourier series (equation 6-14).

$$\begin{aligned}
G_{ij}^n(\theta, \varphi) &= \sum_n^L a_n^n(\theta) \cos[n(\varphi - \alpha)] + b_n^n(\theta) \sin[n(\varphi - \alpha)] \\
\phi &= k_r^n r \cos(\varphi - \alpha) + k_3^n |z| = c^n |z| + g^n \cos[B^n - (\varphi - \alpha)] \\
g^n &= [(k_r^n r + d^n |z|)^2 + (e^n |z|)^2]^{0.5} \\
B^n &= \arctan\left(\frac{e^n |z|}{k_r^n r + d^n |z|}\right)
\end{aligned} \tag{6-14}$$

Since the analytical formula of phase velocity is not available for media under initial stress, the vertical and horizontal wave-number is present as equation 6-15.

$$\begin{aligned}
k_3^n &= \frac{\omega \cos \theta}{V^n(\theta, \varphi)} \quad k_r^n = \frac{\omega \sin \theta}{V^n(\theta, \varphi)} \\
\theta &= \arctan\left(\frac{r}{z}\right)
\end{aligned} \tag{6-15}$$

I did not expand the horizontal wave-number into the first-order Fourier series in order to stay in the same formula in Tsvankin and Chesnokov (1990). As have been tested, this will slightly harm the solution. This error will be discussed in detail in the following sections.

The third integral over k_r can be reduced by the stationary phase approximation. And the last integral over angular frequency ω can be solved by considering the Dirac delta. For the more detailed discussion about this method, the readers may refer to the previous sections or Tsvankin and Chesnokov (1990).

7 Green-Christoffel and the plane wave in pre-stressed medium

7.1 Stiffness tensor

Equation 6-7 can be reduced and written into a second rank symmetric tensor in equation 7-1 according to Liao *et al.* (personal communication, 2010).

$$T_{ij} = \begin{bmatrix} C_{11} & \lambda - \nu_1 t_{33}^0 & \lambda - \nu_1 t_{22}^0 & \nu_1 t_{23}^0 & (\nu_1 + \nu_2) t_{13}^0 & (\nu_1 + \nu_2) t_{12}^0 \\ & C_{22} & \lambda - \nu_1 t_{11}^0 & (\nu_1 + \nu_2) t_{23}^0 & \nu_1 t_{13}^0 & (\nu_1 + \nu_2) t_{12}^0 \\ & & C_{33} & (\nu_1 + \nu_2) t_{23}^0 & (\nu_1 + \nu_2) t_{13}^0 & \nu_1 t_{12}^0 \\ & & & \mu - \frac{1}{2} \nu_2 t_{11}^0 & \frac{1}{2} \nu_2 t_{12}^0 & \frac{1}{2} \nu_2 t_{13}^0 \\ & & & & \mu - \frac{1}{2} \nu_2 t_{22}^0 & \frac{1}{2} \nu_2 t_{23}^0 \\ & & & & & \mu - \frac{1}{2} \nu_2 t_{33}^0 \end{bmatrix} \quad (7-1)$$

$$C_{\alpha\alpha} = \lambda + 2\mu + 2(\nu_1 + \nu_2)t_{\alpha\alpha}^0, \quad \alpha = 1, 2, 3$$

There are only five independent elements in the deviatoric stress (trace must be zero). As well as Lam é parameters, there are seven independent elements. In the case of uniaxial stress along the principal axis of the medium, the above formula can be further simplified (equation 7-2).

$$T_{ij} = \begin{bmatrix} C_{11} & \lambda - v_1 t_{33}^0 & \lambda - v_1 t_{22}^0 & 0 & 0 & 0 \\ & C_{22} & \lambda - v_1 t_{11}^0 & 0 & 0 & 0 \\ & & C_{33} & 0 & 0 & 0 \\ & & & \mu - \frac{1}{2} v_2 t_{11}^0 & 0 & 0 \\ & & & & \mu - \frac{1}{2} v_2 t_{22}^0 & 0 \\ & & & & & \mu - \frac{1}{2} v_2 t_{33}^0 \end{bmatrix} \quad (7-2)$$

$$C_{\alpha\alpha} = \lambda + 2\mu + 2(v_1 + v_2)t_{\alpha\alpha}^0, \quad \alpha = 1, 2, 3$$

7.2 Phase velocity

I will start from equation 7-3 which is the homogeneous equation for the plane wave in pre-stressed medium.

$$\rho_0 \frac{\partial^2 u_i}{\partial t^2} = \tau_{jl}^0 \frac{\partial^2 u_i}{\partial a_l \partial a_j} + T_{ijkl} \frac{\partial^2 u_k}{\partial a_l \partial a_j} \quad (7-3)$$

In the same manner described in the previous sections, the Green-Christoffel equation 7-4 can be found, where c is the phase velocity. Due to the complexity of the initial stress, the phase velocity is usually solved by the numerical method.

$$[(\rho_0 c^2 - \tau_{jl}^0 n_j n_l) \delta_{ik} - T_{ijkl} n_j n_l] u_k = 0 \quad (7-4)$$

7.3 Calculated velocities for different models

The initial deviatoric stress is presented as equation 7-5. I consider a simplified case when the magnitudes of all the elements in stress tensor are equal.

$$t_{ij}^0 = bA_{ij} \quad (7-5)$$

According to Nikitin and Chesnokov (1981), the uniaxial stress can be present as equation 7-6.

$$t_{ij}^0 = a \begin{bmatrix} \sin^2 \psi \cos^2 \vartheta - \frac{1}{3} & \frac{1}{2} \sin^2 \psi \cos 2\vartheta & \frac{1}{2} \sin 2\psi \cos 2\vartheta \\ \frac{1}{2} \sin^2 \psi \cos 2\vartheta & \sin^2 \psi \sin^2 \vartheta - \frac{1}{3} & \frac{1}{2} \sin 2\psi \sin \vartheta \\ \frac{1}{2} \sin 2\psi \cos 2\vartheta & \frac{1}{2} \sin 2\psi \sin \vartheta & \cos^2 \psi - \frac{1}{3} \end{bmatrix} \quad (7-6)$$

“a” is an arbitrary number. Ψ and θ are the Euler angles corresponded to the orientation of the axis of stress.

The elastic constants of the background medium in Table 7-1 and the four types of uniaxial initial stress in Table 7-2 will be used to calculate the radiation patterns and synthetic seismograms.

Background Medium	Additional Parameters
$\lambda = 10 \text{ GPa}$	$b = 1 \text{ GPa}$
$\mu = 9 \text{ GPa}$	$v_1 = 1$
$\rho = 2.5 \text{ g/cc}$	$v_2 = 1$

Table 7-1, Parameters for the background model

Model	Pressure	Matrix “ A_{ij} ”
#1	0	$A_{11} = A_{22} = 0.5; A_{33} = -1;$
#2	-1 GPa	$A_{11} = A_{22} = 0.5; A_{33} = -1;$
#3	0	$A_{11} = A_{22} = -0.5; A_{33} = 1;$
#4	0	$A_{22} = A_{33} = 0.5; A_{11} = -1;$

Table 7-2, Parameters for different initial stress model

It is assumed that the parameters in Table 7-1 are constants throughout the different initial pressures. However, this is not realistic since they should depend on the pressure (equation 6-7). The reason for doing this is that I want to separate the contribution of initial pressure since it appears explicitly in equation 6-9 and 6-10. In the real case, the parameters in Table 7-2 may increase or decrease according to the change of initial pressure and the effect will be more significant than the following results.

The three resulting stiffness are shown in equations 7-7-a, 7-7-b, and 7-7-c. As have been mentioned before, since the influence of initial pressure on the stiffness is excluded, the results for the first two models are same. The first three vertical uniaxial stresses can result in the VTI symmetry while the horizontal uniaxial stress (model four) will produce the HTI (horizontal transversely isotropic) symmetry.

$$C = \begin{bmatrix} 30 & 11 & 9.5 & 0 & 0 & 0 \\ 9 & 30 & 9.5 & 0 & 0 & 0 \\ 9.5 & 9.5 & 24 & 0 & 0 & 0 \\ 0 & 0 & 0 & 8.75 & 0 & 0 \\ 0 & 0 & 0 & 0 & 8.75 & 0 \\ 0 & 0 & 0 & 0 & 0 & 9.5 \end{bmatrix} \quad (7-7-a)$$

$$C = \begin{bmatrix} 26 & 9 & 10.5 & 0 & 0 & 0 \\ 9 & 26 & 10.5 & 0 & 0 & 0 \\ 10.5 & 10.5 & 32 & 0 & 0 & 0 \\ 0 & 0 & 0 & 9.25 & 0 & 0 \\ 0 & 0 & 0 & 0 & 9.25 & 0 \\ 0 & 0 & 0 & 0 & 0 & 8.5 \end{bmatrix} \quad (7-7-b)$$

$$C = \begin{bmatrix} 24 & 9.5 & 9.5 & 0 & 0 & 0 \\ 9.5 & 30 & 11 & 0 & 0 & 0 \\ 9.5 & 11 & 30 & 0 & 0 & 0 \\ 0 & 0 & 0 & 9.5 & 0 & 0 \\ 0 & 0 & 0 & 0 & 8.75 & 0 \\ 0 & 0 & 0 & 0 & 0 & 8.75 \end{bmatrix} \quad (7-7-c)$$

The first stress model will relax the model along the Z-axis. Equation 7-7-a is the VTI medium which is often encountered in the seismology where the largest phase velocities are in the isotropic plane. And the elastic wave whose amplitude is polarized within the isotropic plane will travel faster.

The phase velocity of the qP- and qSV-wave for model one are plotted in figure 7-1. They display the anisotropic property as described above. The results for model two are plotted with the manner in figure 7-2. Comparing with model one, both phase velocities increased due to presence of the compacting initial pressure.

However, the stiffness tensor in equation 7-7-b will have a different impact on the elastic wave propagation. In this case, the direction of the largest phase velocity is along the axis of symmetry and the phase velocity of qSV-wave is usually faster. This is because that the initial stress is compacting along the vertical direction. Due to this reason, the body waves that polarized in the radial plane will travels faster. Without considering the stress, this type of symmetry can be caused by the aligned vertical cracks distributed symmetrically besides the vertical axis – which is often rare to be observed. The calculated phase velocities are plotted in figure 7-3.

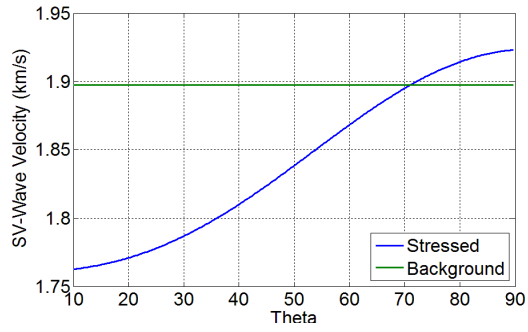
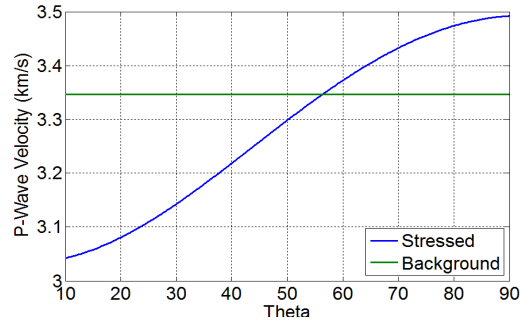


Figure 7-1, Phase velocities of qP- and qSV-wave in stress model one.

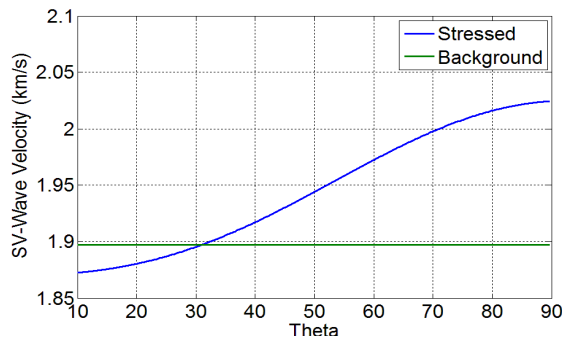
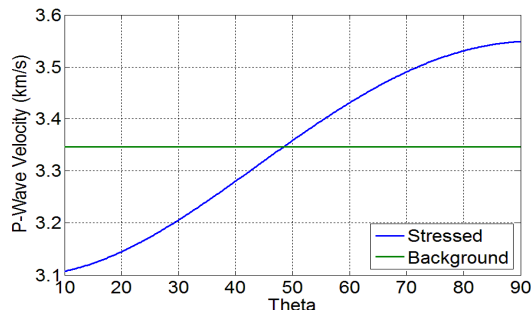


Figure 7-2, Phase velocities of qP- and qSV-wave in stress model two.

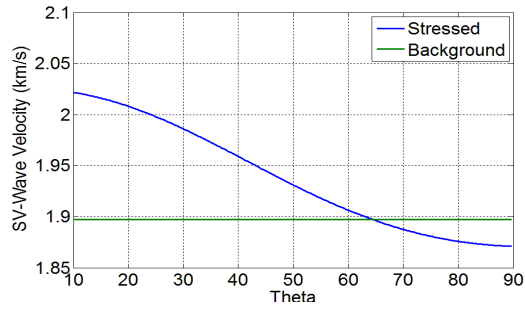
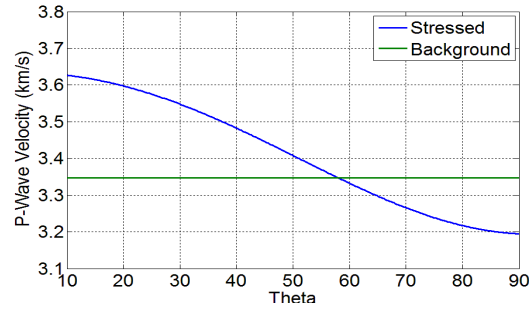


Figure 7-3, Phase velocities of qP- and qSV-wave in stress model three.

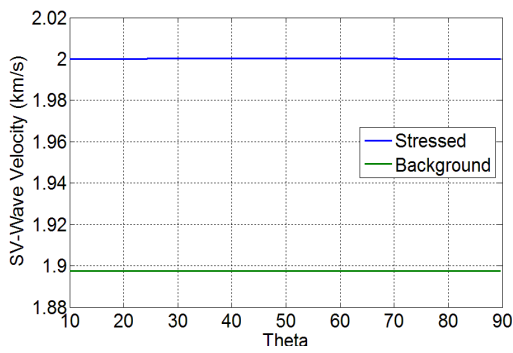
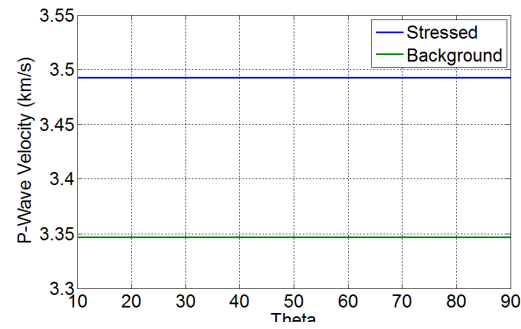


Figure 7-4, Phase velocities of qP- and qSV-wave in stress model four.

Model four was shown in equation 7-7-c. This is a medium of hexagonal symmetry whose symmetric axis is along X-axis. The deviatoric stress is expanding the medium along the symmetric axis. In HTI media like this, the phase velocity varies with different azimuth angles and the largest phase velocity can be found along the isotropic plane (Y-Z plane). In this case, the qSV-wave usually travels faster.

I only show the phase velocities in the symmetry plane (figure 7-4). They are slightly higher than the background velocity due to the compaction within this plane.

8 Synthetic results – radiation patterns and synthetic seismograms

In this section, the radiation patterns and synthetic seismograms are calculated. Lastly, the error in the calculation is studied and discussed.

8.1 Radiation patterns

Figures 8-1 to 8-4 show the radiation patterns of qP- (a) and qSV-wave (b) in the four different models. I only show the results of G_{33} .

There are several reasons causing the distortion of radiation patterns. The first and the biggest impacts are from the phase velocity, since it appears in the Green's tensor directly ($G_{ij} \sim \frac{1}{v^2}$). Secondly, the polarization of the amplitude for body waves in the anisotropic media will tilt from the pure modes.

Figure 8-1 (a) and (b) shows the results in model one. They are similar with the radiation patterns calculated by the stiffness tensor in equation 7-7-a. The difference comes from the Lagrangian wave equations 6-9 and 6-10 that there is an additional term related with the initial stress. This is one of the unique properties for the pre-stressed media.

Comparing figures 7-1 and 7-2, it can be seen that adding the “compacting” initial pressure will generally increase the phase velocities of both qP- and qSV-wave. This will

make the radiation patterns in the compacted media to shrink (figures 8-2-a and 8-2-b). However, the overall anisotropic property is not changing. For this study, the contribution from initial pressure only lies in the additional term in wave equations.

Figures 8-3-a and 8-3-b show the results from an uncommon type of VTI medium. The radiation patterns (figure 8-3) are different from the ones in model one (figure 8-1) but still follow the trend of phase velocities.

I calculate the result in isotropic plane (90 degree azimuth) for model four. In the symmetric plane, both the qP- and qSV-wave become pure modes. The resulting radiation patterns are plotted in figures 8-4-a and 8-4-b. They are very similar to the isotropic radiations except the phase velocities are different.

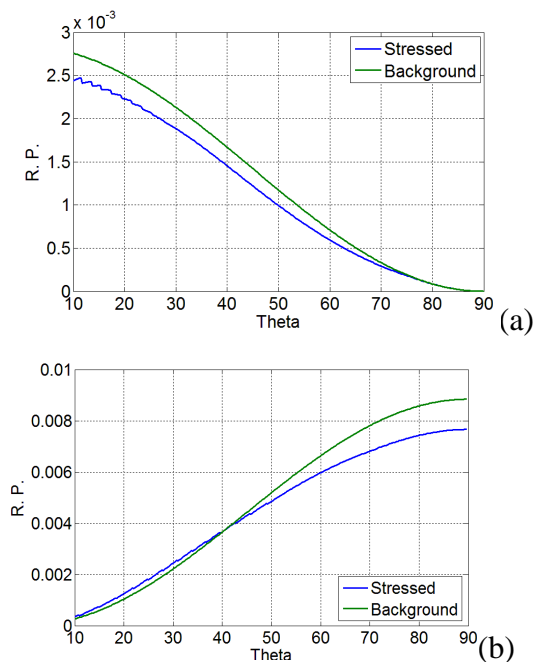


Figure 8-1, Radiation patterns for qP- and qSV-wave in stress model one.

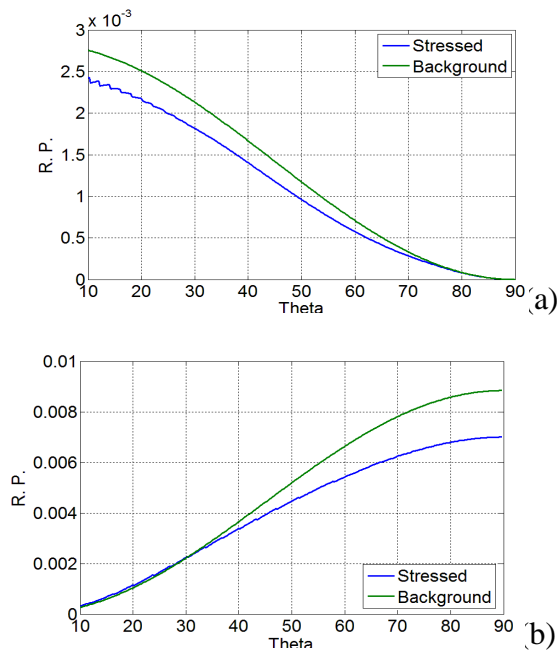


Figure 8-2, Radiation patterns for qP- and qSV-wave in stress model two.

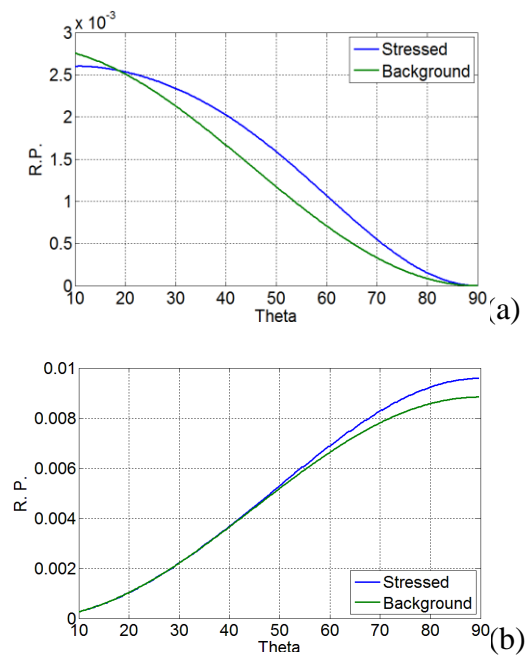


Figure 8-3, Radiation patterns for qP- and qSV-wave in stress model three.

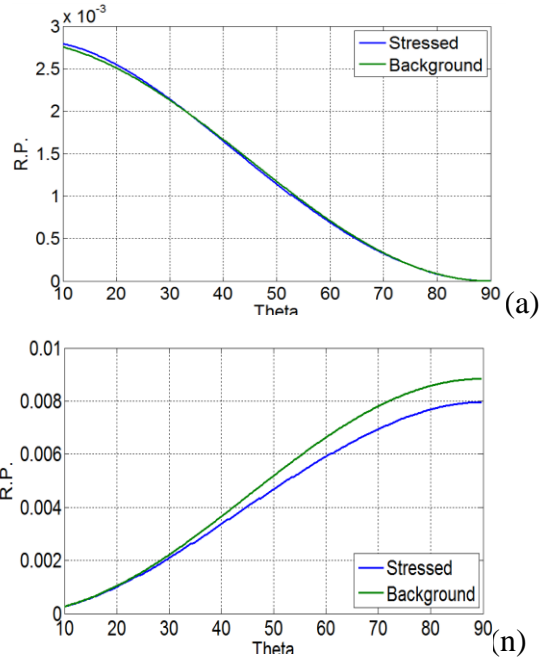


Figure 8-4, Radiation patterns for qP- and qSV-wave in stress model four.

8.2 Synthetic seismogram

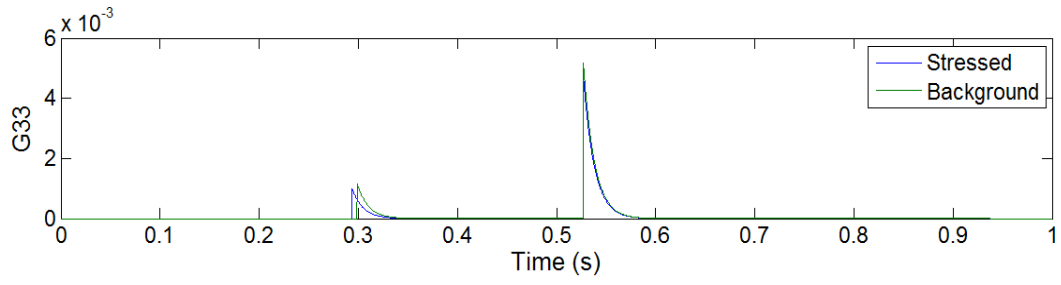
In this section, I calculate the synthetic seismograms corresponded to the four models in Tables 7-1 and 7-2. The receivers are located along the unit radius with different azimuth and polar angles.

The results of the vertical component of receivers are calculated and showed in figures 8-5 to 8-8. I consider a vertical source and the wavelet described in equation 4-6. The x component seismograms from the x-force are shown in figure 8-9 only for model four. The azimuth is 90 degrees thus there are only SH waves.

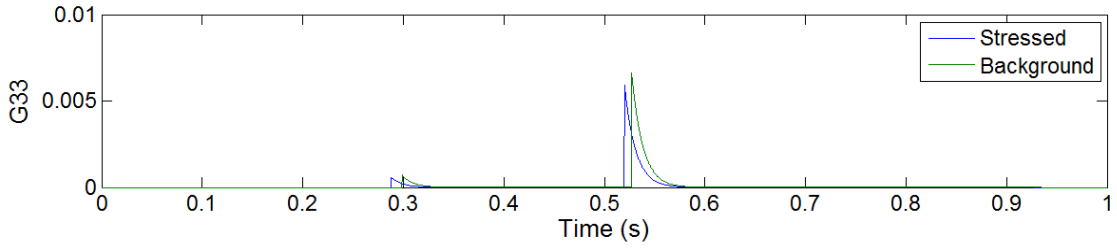
For the first three types of model with VTI symmetry, the amplitude is following the radiation patterns calculated in the above section. The group velocity is approximated by the

stationary phase points (figures 8-5 to 8-8).

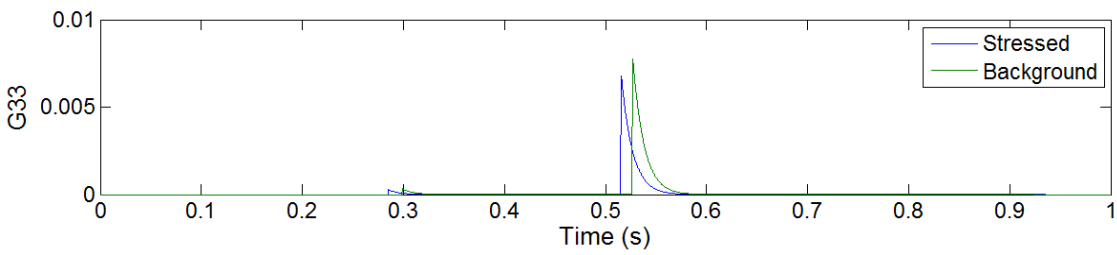
The time arrivals of both phases are slightly changing in the seismograms from model four. This is not correct due to the fact that the receivers are set in the isotropic plane. In the isotropic plane, the phase velocity should be same with group velocity. Thus there is a chance for one to evaluate the error by finding the difference in theoretical and calculated time arrival. In this way, I study the effect of neglecting the high-order terms in the horizontal slowness.



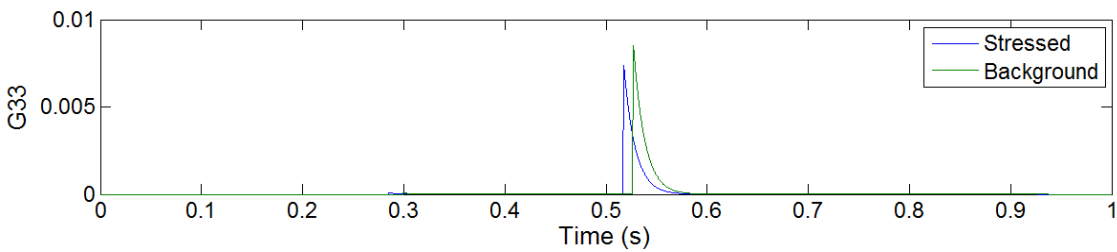
(a)



(b)

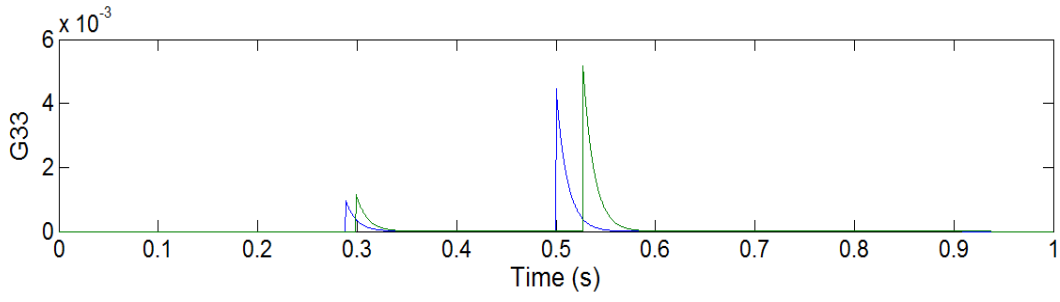


(c)

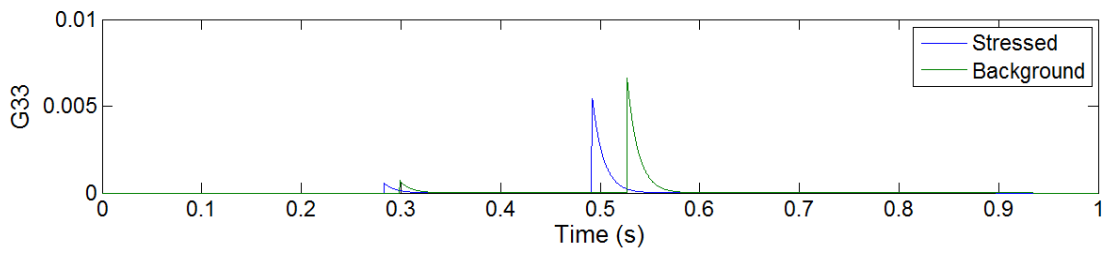


(d)

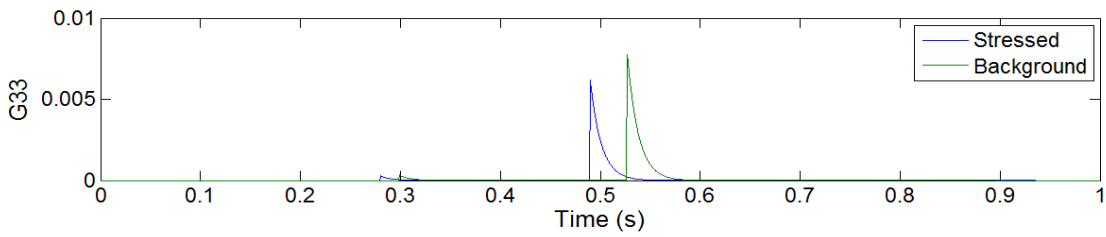
Figure 8-5, Synthetic seismograms at azimuth=90 and theta=50, 60, 70, 80 (from top to bottom) in stress model one.



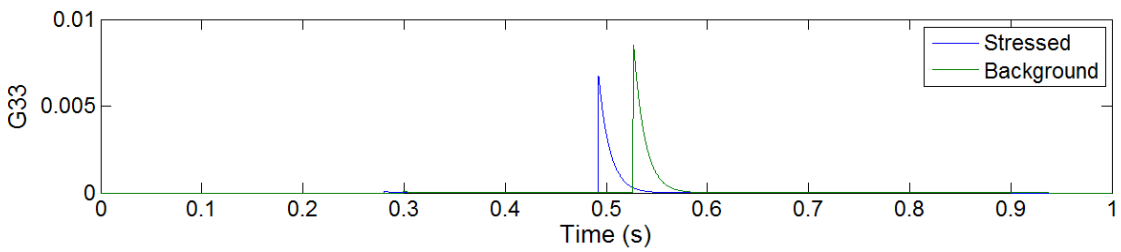
(a)



(b)



(c)



(d)

Figure 8-6, Synthetic seismograms at azimuth=90 and theta=50, 60, 70, 80 (from top to bottom) in stress model two.

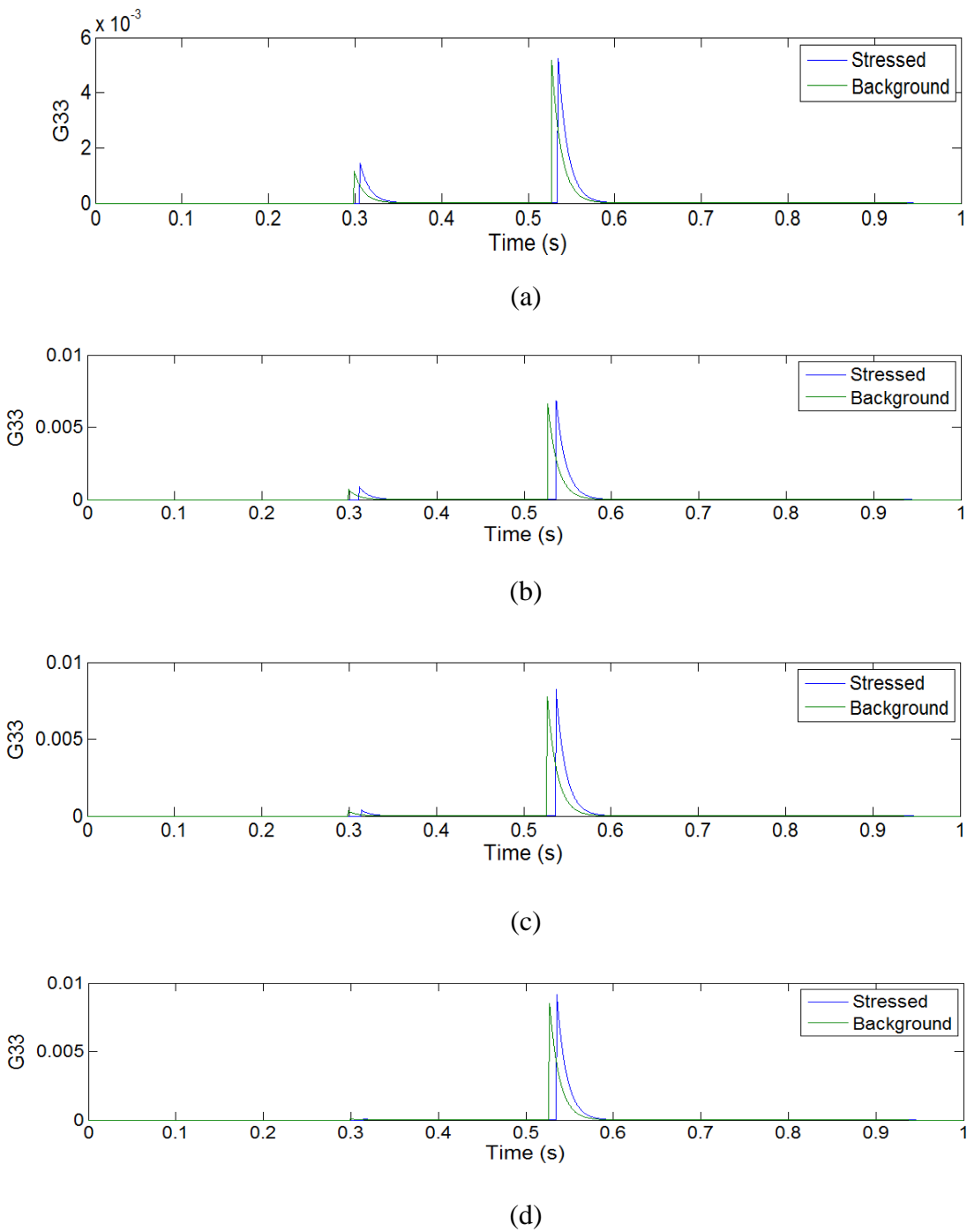
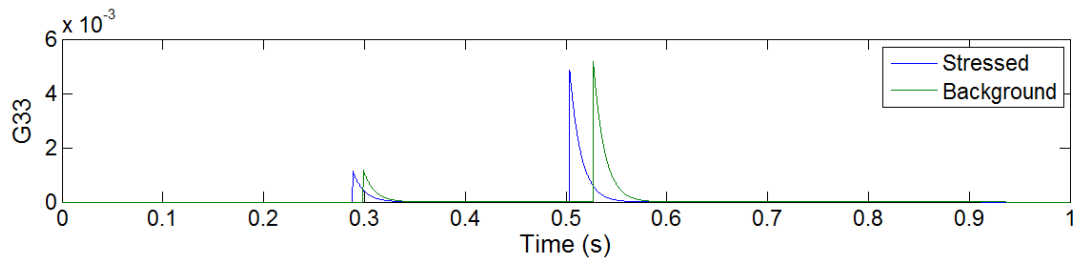
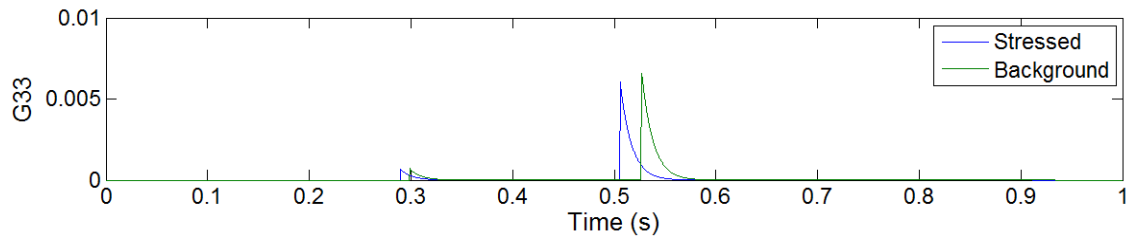


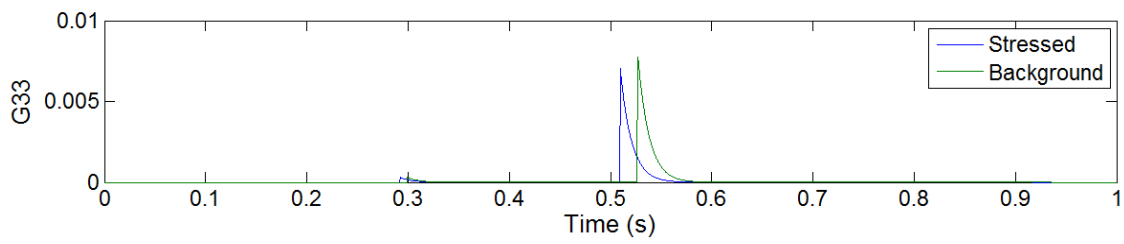
Figure 8-7, Synthetic seismograms at azimuth=90 and theta=50, 60, 70, 80 (from top to bottom) in stress model three.



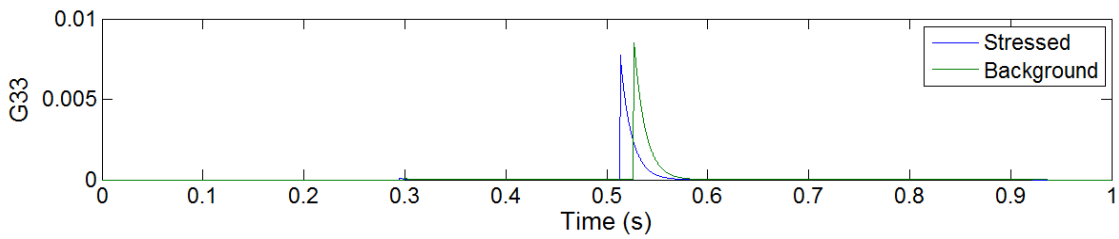
(a)



(b)



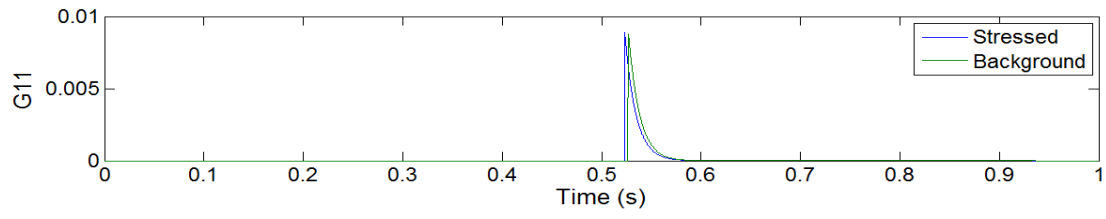
(c)



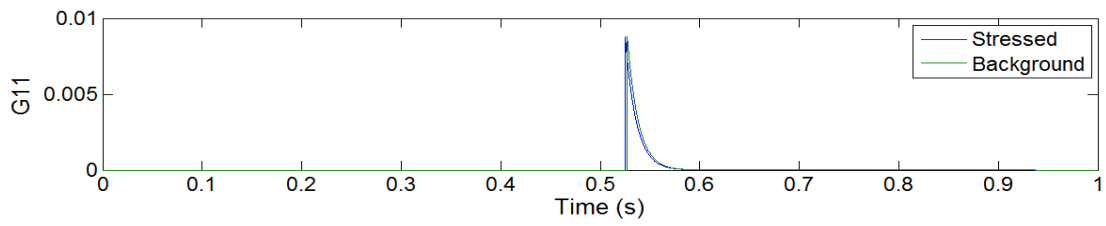
(d)

Figure 8-8, Synthetic seismograms at azimuth=90 and theta=50, 60, 70, 80 (from top to

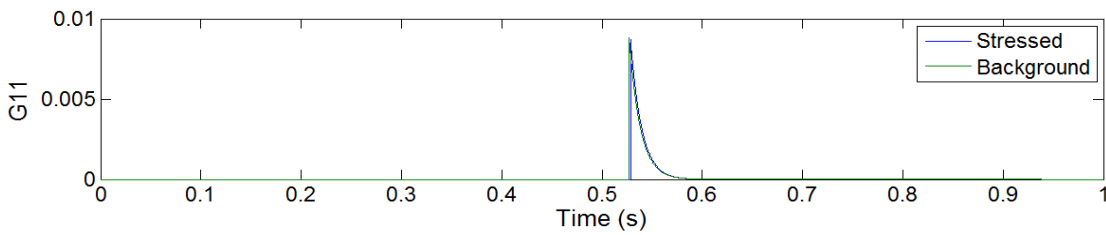
bottom) in stress model four.



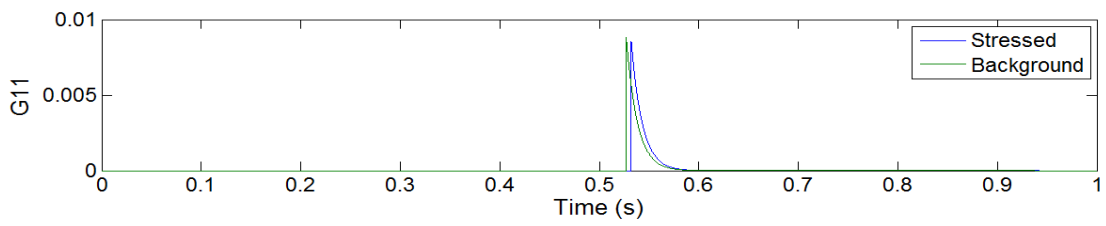
(a)



(b)



(c)



(d)

Figure 8-9, Horizontal component synthetic seismograms

at azimuth=90 and theta=50, 60, 70, 80 (from top to bottom) in stress model four.

$$O = \frac{t_{true} - t_{cal}}{t_{true}} \cdot 100\% \quad (8-1)$$

Theta	Error in time arrival P-wave (in %)	SV-wave (all absolute value)	SH-wave
50	0.8	0.7	0.6
60	1.2	1.2	1.0
70	2.0	1.9	1.65
80	2.8	2.7	2.3

Table 8-1, Error in time arrival calculated for stress model four.

I define the relative error of time arrivals by equation 8-1. The calculated errors are shown in Table 8-1. This error is due to several reasons. The biggest one is the expanded parts in horizontal slowness is neglected; therefore, the error is increasing towards the horizontal axis. Since the horizontal slowness is increasing, the part being neglected will also become bigger, thus leads to bigger errors. The error is also linked with the property of the initial stress. For the stronger azimuthally anisotropic model, this error may increase accordingly.

9 Conclusion for Part II

In this part, the elastodynamic Green's tensor in the pre-stressed medium is calculated when the background medium is isotropic and the initial stress tensor is homogeneous. The deviatoric part of initial stress will alter the symmetry of the medium while the pressure will contribute to the value of the elastic parameters.

Besides the anisotropic effect, the Green's tensor in Lagrangian wave equation will behave differently due to the additional term in the wave equation which is linked with the initial stress tensor directly. This term will not change the symmetry of the medium but will contribute to the overall magnitude of the phase velocity, thus the Green's tensor.

The error is introduced since I drop the azimuthally dependent part of horizontal slowness in the process of calculating the inverse Fourier transform. The error will become bigger toward the horizontal plane (X-Y plane) and will increase along with the azimuthally anisotropic property of the medium.

10 Reference

Ben-Menahem, A., and Sena A. G., 1990, Seismic source theory in stratified anisotropic media: *J. Geophys. Res.*, 95, (15), 395–15427.

Biot, M. A., 1940, The influence of initial stress on elastic waves: *Journal of Applied Physics*, 11, (8), 522-530.

Bland, D. R., 1969, *Nonlinear dynamic elasticity*: Blaisdell Publishing Company, p.1-94.

Bleistein, N., 1984, *Mathematical methods for wave phenomena*: Academic Press.

Christoffel, E.G., 1877, Uber die Fortpflanzung von Stossen durch elastische feste Korper: *Ann. di Mat.*, 8, 193-243.

Dahlen, F. A., 1972, Elastic dislocation theory for a self-gravitating elastic configuration with an initial static stress field: *Geophys. J. Roy. Astr. Soc.*, 28, (4), 357–383.

Daley, P. F., and Hron, F., 1977, Reflection and transmission coefficients for transversely isotropic media: *Bull. Seism. Soc. Am.*, 67, 661-675

Dellinger, J. A., 1991, *Anisotropic seismic wave propagation*, Phd Thesis, Stanford University.

Gajewski, D., 1993, Radiation from point sources in general anisotropic media: *Geophys. J. Int.*, 113, 299–317.

Gridin, D., 2000, Far-field asymptotics of the Green tensor for a transversely isotropic solid. *Proc. R. Soc. A* 456, 571 - 591.

Nikitin, L. V., and Chesnokov, E. M., 1981, Influence of a stress condition on the anisotropy of elastic properties in a medium: *Izv. Earth Physics*, 17, (3), 174-183.

Nikitin L.V., and Chesnokov, E.M., 1984. Wave propagation in stress induced media: *Geoph.J.R.astr. Soc.* 76, 129-133.

Stokes, G. G., 1849, On the dynamical theory of diffraction: *Trans. Camb. Phil. SOC.*, 9, 1-62.

Ting, T. C. T., 1996, *Anisotropic elasticity: theory and application*: Oxford University Press

Tsvankin, I. D., and Chesnokov, E. M., 1990, Synthesis of body wave seismograms from point sources in anisotropic media: *Journal of Geophysical Research*, 95, (B7), 11317-11331

Tsvankin, I., and Thomsen, L., 1994, Nonhyperbolic reflection moveout in anisotropic media: *Geophysics*, 59, 1290-1304.

Tsvankin, I., 1995, Body-wave radiation patterns and AVO in transversely isotropic media: *Geophysics*, 60, 1409-1425.

Tsvankin, I., 1996, P-wave signatures and notation for transversely isotropic media: An overview: *Geophysics*, 61, 467-483

Vavryčuk, V., and Yomogida, K., 1996, SH-wave Green tensor for homogeneous transversely isotropic media by higher-order approximations in asymptotic ray theory: *Wave Motion*, 23, 83-93.

Vavryčuk, V., 1997, Elastodynamic and elastostatic Green tensors for homogeneous weak transversely isotropic media: *Geophys. J. Int.*, 130, 786-800.

Vavryčuk, V., 2002, Asymptotic elastodynamic Green function in the kiss singularity in homogeneous anisotropic solids: *Stud. Geophys. Geod.*, 46, 249-266.

Vshivtsev, A. S., Zhukowskii, K. V., and Chesnokov, E. M., 1996, An effect of initial non uniform stresses on the elastic properties of an anisotropic body: *Physics of the Solid Earth, English Translation*, 31, (5), 429-436.